MODELING CHALCOPYRITE LEACHING KINETICS

by

JAIME TREJO GALLARDO

B.Sc., Universidad Autonoma Metropolitana, 2004

A THESIS SUBMITTED IN PARTIAL FULFILLMENT
OF THE REQUIREMENTS FOR THE DEGREE OF
MASTER OF APPLIED SCIENCE

in

THE FACULTY OF GRADUATE STUDIES
(Materials Engineering)

THE UNIVERSITY OF BRITISH COLUMBIA

December 2007

ABSTRACT

Chalcopyrite ($CuFeS_2$) is the most abundant of the copper sulfides and also one of the most refractory for leaching. Several processing routes have been proposed to overcome drawbacks associated with environmental problems related to copper extraction from this mineral. Atmospheric leaching in acidic ferric sulfate is regarded as being particularly attractive over other hydrometallurgical systems. However, the challenge has been to overcome the problem of slow extraction rates due to passivity encountered at high solution potentials in this system. This highlights the need to investigate better operating conditions to optimize copper extraction and prevent the problem of passivation, and to develop suitable modeling tools to assess and diagnose leaching performance.

In this work, a dissolution rate expression for chalcopyrite leaching in acidic ferric sulfate media is proposed accounting for effects in the active and passive regions under potentials from 415 to 550 mV (Ag/AgCl). A model of chemical speciation in the bulk solution elucidates the idea of passivation caused by precipitation of ferric species and their consequent adsorption onto the chalcopyrite surface. Electrochemical studies on massive samples of chalcopyrite involving characterization and modeling of the anodic and cathodic half-cell reactions of chalcopyrite leaching together with mixed potential considerations lead to the development of the mathematical expression for dissolution rate.

The mathematical model was calibrated with electrochemical parameters and results are in good agreement with real leaching data from batch tests for solution potential regions where passivity is not observed. On the other hand, the passive region was modeled by means of adjusting parameters related to adsorption energies of the passivating species. Results of the model for this region deviate from real data as potential becomes higher probably due to diffusion resistance through a layer composed of ferric complexes.

TABLE OF CONTENTS

LIST OF TABLES

LIST OF FIGURES

CHAPTER 1 INTRODUCTION

Hydrometallurgy represents a potentially attractive alternative to pyrometallurgy for the extraction of metals. Recent developments in copper hydrometallurgy reflect in the desire to create economically viable alternatives to smelting, with its itinerant environmental and economic drawbacks, including (Ballester et al., 2005; Dreisinger, 2006):

- Toxic SO_2 emissions
- Sulfuric acid market saturation
- High capital and operating costs
- Limitations related to the presence of other metal impurities

Problems associated with the chemical and electrochemical nature of hydrometallurgical operations and subsequent stages of processing have resulted in economic failure for many emerging processes. Thus, smelting still accounts for over 80% of all copper production (Ballester et al., 2005), while hydrometallurgical treatment is largely confined to oxide ores and secondary sulfides such as chalcocite and covellite. The knowledge gained from the study of those minerals has been widely applied in heap and tank leaching operations, allowing efficient treatment of secondary copper ores.

Chalcopyrite, the most abundant copper-bearing mineral, is known to be recalcitrant to dissolution, and much research has been conducted to solve the difficulties that hinder its viable exploitation (Davenport et al., 1976). In efforts to provide the copper industry with an efficient way to recover copper from chalcopyrite ores, various dissolution processing options based on different chemical systems have been proposed (Dreisinger, 2006). Among them, the H_2SO_4-$FeSO_4$-$Fe_2(SO_4)_3$-H_2O system in particular remains very attractive because the strong oxidizing potential attained with ferric sulfate solutions is enough to oxidize a good number of metal sulfides including chalcopyrite (Gupta and Mukherjee, 1990). Also, this chemical system is inexpensive (since the required iron and acid come from the oxidation of the minerals themselves, and the ferric oxidant is readily regenerated with oxygen gas), and only mildly corrosive. As a

result of these advantages, the H_2SO_4-$FeSO_4$-$Fe_2(SO_4)_3$-H_2O system has found broad application to the processing of many sulfide ores.

It is clearly accepted that chalcopyrite undergoes passivation at certain ferric concentrations, thus resulting in low extraction rates (Hackl et al., 1995; Kametani and Aoki, 1985). Understanding the mechanism of, and knowing the conditions which lead to, this passivity is the key to developing leaching routes that can lead to efficient ways of copper extraction by ferric ions, and to designing methods to control those variables which influence this passivity (Dixon and Petersen, 2002).

From this perspective, there exists a definite need to develop mathematical models for the grain-scale leaching of chalcopyrite with direct application to commercial-scale leaching systems. Several kinetic expressions representing chalcopyrite leaching in the H_2SO_4-$FeSO_4$-$Fe_2(SO_4)_3$-H_2O system to forecast extraction levels have been proposed in the past. However, applicability of those models has been very limited.

This study establishes the methodology for obtaining an intrinsic kinetic model for chalcopyrite dissolution in the acidic ferric sulfate system, incorporating the principles of electrochemical kinetics as a mathematical basis.

Thermodynamics of the H_2SO_4-$FeSO_4$-$Fe_2(SO_4)_3$-H_2O system are modeled to provide a quantitative explanation of passivity based on the adsorption of ferric precipitates whose stability depends on solution potential. Modeling this adsorption process is necessary for the mathematical description of passivation. A comprehensive kinetic study is comprised of chemical characterization involving potential-controlled tank leaching experiments to obtain kinetic parameters under a wide range of solution potentials, and electrochemical characterization conducted separately to elucidate the effects of passivity related to redox potential. The kinetic expression derived accounts for the common dissolution mechanism observed for other sulfides in the active potential region, as well as the passivity observed specifically for chalcopyrite at higher potentials.

CHAPTER 2 LITERATURE SURVEY

Emerging technologies for the profitable exploitation of primary copper minerals (particularly chalcopyrite) have necessitated a fundamental understanding of the processes by which these minerals are extracted. This understanding involves the investigation of physical and chemical mechanisms under which chalcopyrite can be efficiently leached and also the development of tools that can aid the modeling and interpretation of the observed phenomena. Acidic ferric sulfate solutions could potentially have broad application for the processing of chalcopyrite ores and concentrates. Thus, various means of promoting more efficient extraction in this medium have been studied in order to better understand the mechanisms of dissolution and to facilitate the optimal selection of operating conditions and processing routes for treatment of chalcopyrite. In this chapter, previous studies concerning the important factors affecting chalcopyrite leaching, and the possible causes and mechanisms of chalcopyrite passivation, are reviewed. Also, the various theories proposed to explain chalcopyrite passivity, and the various kinetic models developed to predict experimentally observed leaching rates, are discussed.

2.1 Factors Affecting Chalcopyrite Leaching Kinetics

Previously, it has been found that temperature, particle size, and oxidant concentration are among the most important variables influencing the rate of chalcopyrite dissolution. Sullivan and Brown (1934), conducted some of the first studies on the general behavior of chalcopyrite leaching by oxidizing finely ground chalcopyrite using a 1% ferric sulfate solution at 35°C. Under those conditions, only 38% of the copper was extracted during 57 days of leaching. They observed improvements in the rate of extraction with increasing temperature, whereby the same level of extraction was achieved in just 5 hours at 35°C. Chalcopyrite dissolution was thought to proceed by two main reactions:

$$CuFeS_2 + 4\,Fe^{3+} \rightarrow Cu^{2+} + 5\,Fe^{2+} + 2\,S^0 \qquad (I)$$

$$4CuFeS_2 + 2\,H_2SO_4 + 17\,O_2 \rightarrow 4\,CuSO_4 + 2\,Fe_2(SO_4)_3 + 2\,H_2O \qquad (II)$$

Most of the copper dissolved according to reaction (I) and the rest according to reaction (II), presumably due to the limited availability of oxygen (Ballester and Cordoba, 2005).

Wadsworth (1972) also studied the ferric sulfate leaching of chalcopyrite and identified particle size as the only controllable variable which had a significant influence on the leaching rate. In his experimental work, ultrafine chalcopyrite at particle size of 0.5 μm was leached with a stoichiometric amount of $Fe_2(SO_4)_3$ dissolved in 1 M H_2SO_4 at 93°C. He attributed the relatively high copper extraction (90% after 3.5 h) to the increased mineral surface area resulting from the ultrafine grinding. On the other hand, Jones and Peters (1976) suggested that chalcopyrite leaching takes place along fissures or grain boundaries and no advantage can be gained by continuing size reduction below 0.5 μm.

The influence of reagents on chalcopyrite leaching has also been studied. According to Hirato et al. (1987), the dissolution rate revealed a significant dependency on ferric concentration at relatively low levels (0.001 to 0.1 M), whereas no dependency was observed at higher concentrations. Dutrizac et al. (1969), studied the leaching of chalcopyrite in acidic solutions, showing that the dissolution rate was enhanced by maintaining low pH. This pH control is critical to avoid hydrolysis and precipitation of ferric salts resulting in the occurrence of jarosites.

2.2 Mathematical Expressions Describing Chalcopyrite Leaching Kinetics

Mathematical expressions describing the rate of chalcopyrite leaching in ferric solutions are generally based on one of two rate limiting mechanisms. Diffusion across the elemental sulfur product layer and the intrinsic rate of oxidation at the mineral surface are considered to be the two most important rate-limiting phenomena to consider in modeling overall leaching kinetics (Bonn and Heijnen, 1993).

Wadsworth (1972) proposed a model for the dissolution of chalcopyrite where the presence of ferric ion at the mineral surface was taken to be dependent on the rate of diffusion through a sulfur film whose thickness was assumed to be proportional to Δn, the amount of copper in solution. His model resulted in the following equation:

$$k_p t = \frac{\Delta n^2}{(1-\alpha\Delta n)} - \frac{1}{\alpha^2(1-\alpha\Delta n) + 4.606\log(1-\alpha\Delta n) - (1-\alpha\Delta n)} \qquad (2.1)$$

where α is a stoichiometric factor and k_p is a parabolic leaching rate constant which is dependent on ferric concentration at low concentrations. At relatively high ferric

concentrations no dependency was observed. This fact was attributed to the formation of strong sulfate complexes in solution diminishing the activity of ferric. Paul et al. (1992) developed a model to evaluate the economic feasibility of recovering copper from porphyry copper sulfide orebodies. Their model incorporated energy balances and reaction kinetics of individual minerals using the following calibrated kinetic expression for chalcopyrite leaching (Munoz et al., 1979; Madsen and Wadsworth, 1981):

$$\frac{d\alpha}{dt} = \frac{0.9269 \exp(-20{,}000/RT)}{r_p^2 \zeta} \frac{(1-\alpha)^{1/3}}{(1-(1-\alpha)^{1/3})} \tag{2.2}$$

where r_p and ζ are the radius and the sphericity factor of the mineral grain, respectively. This expression was derived based on consideration of the Wagner theory of oxidation, which suggests that the rate limiting process is the transport of electrons through the elemental sulfur layer. Reaction kinetics were found to be independent of $Fe_2(SO_4)_3$ concentration in the range of 0.06 to 0.5 M and the role of H_2SO_4 was only to prevent the hydrolysis of ferric. Although chalcopyrite leaching is not explicitly accounted for in their model, Ogbonna et al. (2005) presented a “universal electrochemical rate law” as part of a general heap bioleaching model incorporating the effect of solution composition in the following form:

$$f(C) = \frac{C_{Fe^{3+}}}{(k_A + C_{Fe^{3+}})^{1-m}(k_B + C_{Fe^{2+}})^m} \tag{2.3}$$

where k_A, k_B and m are adjustable parameters depending on the electrochemical nature of the mineral dissolution reaction. Upon a suitable estimation of parameters, the model sufficiently reproduces the results of leaching kinetics for non-passivating sulfides such as chalcocite. In the case of chalcopyrite leaching, this model lacks the power to reproduce leaching results when passivity is encountered.

There have been other attempts to better understand and model chalcopyrite kinetics in bioleaching systems. Dixon and Petersen (2002) obtained good copper extraction results for chalcopyrite bio-oxidation in column leaching experiments using concentrates coated onto inert support rocks. Later, Petersen and Dixon (2006) remarked on the importance of the fundamentals of the ferric oxidation of sulfide minerals and their repercussions in bioleaching kinetics. While their observations did not lead them to a

definitive model of chalcopyrite leaching including passivation, they did propose an empirical rate expression based on the assumption that chalcopyrite leaching comprises the sum of two parallel reactions, the prevalence of which switches around some critical ferric-to-ferrous ratio R_{crit} beyond which passivation begins to occur:

$$\frac{dX}{dt} = R^{0.5}\left\{A\exp\left(\frac{-R}{R_{crit}}\right) + B\left[1-\exp\left(\frac{-R}{R_{crit}}\right)\right]\right\} f(X) \tag{2.4}$$

where $R = \frac{C_{Fe^{3+}}}{C_{Fe^{2+}}}$

Although this expression for chalcopyrite conversion is still subject to the estimation of empirical parameters *A* and *B* which are functions of temperature, the model is capable of emulating mathematically the mechanisms of passivity in accordance with Hiroyoshi et al. (2000).

2.3 Modeling Passivity and the Role of Potential in Chalcopyrite Kinetics

Regardless of its nature, passivity is directly responsible for diminishing the rate of chalcopyrite dissolution. Hence, the appropriate modeling of chalcopyrite kinetics must incorporate the effects of this important phenomenon under the relevant conditions.

2.3.1 Advances in modeling chalcopyrite passivity

Passivation is an important fact in the corrosion of metals which has been explained by many researchers. Griffin (1984) presented a kinetic model describing the passivation of metal surfaces due to adsorbed cations produced form the surface oxidation of metal. He proposed a dissolution rate of those cations as a function of the coverage and energy associated with subsequent cation desorption. Rush and Newman (1995) interpreted passivation of iron in sulfuric acid media, where precipitated salt film was believed to be a precursor to oxide passivation and an effective passivation species itself.

Dissolution kinetics using electrochemical techniques have also been studied for metals undergoing passivity. In the work of Jansen and Beck (1995), a kinetic model was developed to characterize zinc oxidation incorporating a charge transfer process and

the transport of anions towards the metal surface through a non-porous passive film of zinc salt. Crundwell and Godorr (1997) developed a mathematical model using mixed potential theory to describe the leaching of gold in cyanide solutions, proposing reaction at the surface as the rate-controlling step. They also accounted for gold passivity by assuming that the active surface area is progressively covered by a passivating layer which grows at a rate proportional to the total amount of surface area available, and which is only dominant during the later stages of leaching.

In the field of mineral sulfide dissolution, research towards the comprehension of passivity in chalcopyrite has led to the development of theories with mathematical models to support their hypotheses and observations. Munoz et al. (1979) studied the kinetics of chalcopyrite dissolution in the acid ferric sulfate media using monosize particles. They attributed passivity to the elemental sulfur product layer. Thus, the rate-limiting step was believed to be the transport process through this layer. Their analysis was supported by the prediction of the empirical activation energy of 83.7 kJ/mol for the transfer of electrons through elemental sulfur. Later, Dutrizac (1989) observed non-linear behavior in leaching of chalcopyrite at various $Fe_2(SO_4)_3$ concentrations (0 to 2 M) at 95°C. He obtained 94% yield of elemental sulfur and 6% SO_4, and these amounts were independent of the leaching time, up to approximately 70 hrs. Passivity was attributed to the formation of large sulfur agglomerates creating a transport barrier.

Stott et al. (2000) attributed passivation of chalcopyrite during bioleaching to the precipitation of iron-hydroxy compounds, indicating that even a thin surface coating of precipitated jarosite is sufficient to diminish the copper leaching rate significantly. Parker et al. (2003) detected several sulfur species on the surfaces of oxidized chalcopyrite residues by means of X-ray photoelectron spectroscopy (XPS), and also attributed passivation to the occurrence of basic ferric sulfate compounds acting as nucleation templates for jarosite formation. This basic ferric sulfate resulted from the oxidative transformation (protonation and hydration) of sulfur species. Later, Sandstrom et al. (2005) confirmed this observation when they analyzed chalcopyrite residues by XPS which had previously been subjected to bacterial and chemical leaching at 420 and 600 mV (Ag/AgCl) and 65°C, finding large amounts of sulfur in both environments at conditions of lower potential. However, higher levels of extraction at 420 mV (compared to 600 mV) and more complete oxidation of sulfur to sulfate were attained in the

bioleaching test, indicating that chalcopyrite passivation was due to jarosite precipitation and not to the elemental sulfur layer. Ballester and Cordoba (2005) carried out chalcopyrite leaching experiments in ferric sulfate media at 68°C and 500 mV (Ag/AgCl), extracting approximately 30% copper, whereas a test at 400 mV yielded nearly 90% extraction during the same leaching time (14 days). They also determined the presence of a passivating layer composed of jarosites hampering ionic species transport to the mineral surface, and found the occurrence of jarosites and the consequent passivity were favored when the redox potential of the leaching slurry exceeded a critical potential value between 400 and 500 mV. Their results were consistent with a theory proposed by Hiroyoshi et al. (2000) suggesting that chalcopyrite is promoted by ferrous in the first stage, involving the reduction to Cu_2S and the subsequent oxidation of this intermediate. Hiroyoshi's leaching model is based on thermodynamic calculations to predict the critical potential being a function of ferrous and cupric concentrations. Regarding the determination of this critical potential, recently Viramontes-Gamboa et al. (2007), with the aid of electrochemical techniques applied on massive mineral samples, developed a procedure to predict the passivation potential of chalcopyrite and to delimit the potential range where chalcopyrite can be leached most effectively.

Other researchers have proposed different mechanisms for chalcopyrite passivity attributed to mineralogical transformations. Hackl et al. (1995) believed that passivity in sulfate media was due to a copper-rich layer formed during the initial stages of leaching. They developed a mixed diffusion-chemical reaction model where the reaction rate was limited by the dissolution of this polysulfide layer. Studies of the electrochemical dissolution of chalcopyrite have helped to elucidate mechanisms of the anodic half-cell reaction where passivity results from the formation of surface films or defect structures of chalcopyrite. Warren et al. (1982) studied the anodic oxidation of chalcopyrite and found the intermediate defect structure $Cu_{1-x}Fe_{1-y}S_{2-z}$ which further decomposed to a second intermediate $CuS_{(n-s)}$, and which he hypothesized to constitute the passivating layer by limiting ionic transport to the active mineral surface. Nava and Gonzalez (2006) also identified different mineral species involved in chalcopyrite surface oxidation, involving the formation of porous layers of non-stoichiometric polysulfides formed after

consecutive mineralogical changes as anodic dissolution progresses from states of low potential to high potential.

2.3.2 Role of solution potential

Passivity seems to be influenced and determined by the solution chemistry wherein species that either promote or are directly responsible for passivity can be identified. Therefore, distribution and concentration of all chemical species determine both the conditions for passivity to occur and the solution redox potential, which is an important factor in the rate of atmospheric ferric-based leaching processes.

Pinches et al. (2001) have developed a process for leaching chalcopyrite by controlling the surface potential (assumed to be equal to the solution redox potential) within an empirically determined window of potentials between 350 and 450 mV (Ag/AgCl). Third et al. (2002) noted the importance of controlling the slurry potential during chalcopyrite bioleaching tests, since final copper extractions from 52 to 61% were achieved compared to tests carried out with a continuous supply of oxygen which yielded less than 30% copper extraction. They also found that potential control helps delay the onset of passivity, provided that a constant redox potential is maintained over the course of leaching. Watling (2006) reviewed all aspects of chalcopyrite bioleaching, concluding that dissolution was sensitive to redox potential, and that basic ferric sulfate phases akin to jarosite could form to hinder further oxidation. Control of solution potential is also important in the measurement of chemical oxidation kinetics with a view to formulating suitable rate laws (Petersen et al., 2005).

From previous research, it can be inferred that chemical mechanisms taking place in the leaching solution seem to be a key factor to prevent or encourage passivity. However, work on modeling the effects of potential and its relationship to passivity for mineral sulfides is very limited in the literature, and mathematical rate expressions considering passivity are still unavailable. In this respect, all important phenomena related to thermodynamics, electrochemistry and passivity of chalcopyrite dissolution have to be embraced and assembled towards the development of an integral reaction rate expression that incorporates the effects of all variables interacting in the H_2SO_4-$FeSO_4$-$Fe_2(SO_4)_3$-H_2O system for the satisfactory modeling of chalcopyrite dissolution.

CHAPTER 3 THEORETICAL DEVELOPMENT

In this chapter the theoretical foundations of all aspects of this study are outlined. The starting point to develop a mathematical model capable of describing the leaching kinetics of chalcopyrite in atmospheric ferric sulfate media is the determination of a rate expression for the dissolution of reacting solids with a leaching solution and the functional relationships of the variables involved. General electrochemical principles used to derive an expression for chalcopyrite dissolution kinetics, and particularly mixed potential considerations, are explored as well in this chapter. This theory has proven valuable for modeling kinetics for other mineral sulfides such as chalcocite (Bolorunduro, 1999) and pyrite (Bouffard et al., 2006). However, mechanisms for chalcopyrite passivity associated with chemical speciation in the bulk solution must be considered in the derivation of a mathematical expression. A comprehensive speciation model based on the work of Casas et al. (2005) is developed to incorporate the effects of important species participating in the chalcopyrite dissolution process. Results from this speciation model will be used in Chapter 5 to model the adsorption of potential passivating species.

3.1 Modeling of Leaching Kinetics

Many particle leaching systems can be modeled by performing differential mass balances on the reacting particle, considering mass transfer and heterogeneous reaction phenomena and the diffusion of products and reactants through porous product layers (Dixon and Dreisinger, 2003). In this work, the shrinking sphere model was employed to represent the leaching of chalcopyrite, assuming the intrinsic rate of heterogeneous reaction at the mineral surface to be the rate limiting step. The expression for the rate of conversion for a single mineral particle takes the following form:

$$1 - X = \left(1 - \frac{t}{\tau}\right)^3 \tag{3.1a}$$

where X is the fractional conversion of the spherical particle, t is time, and τ is the timescale of the reaction. Assuming surface reaction as the rate-limiting step, the timescale takes the following form:

$$\tau = \frac{D}{k \cdot f(C)} \tag{3.1b}$$

Equation 3.1b corresponds to the basic general form of the timescale for a heterogeneous reactive system involving a kinetic constant *k*, leaching particles of initial diameter *D*, and with a dependency on reactant concentrations *f*(*C*).

In this specific case, the timescale τ is taken as the theoretical time required to leach a particle to completion (Dixon and Dreisinger, 2003). Within this parameter, all kinetic aspects of the dissolution reaction are confined. The most important variables affecting this timescale are temperature, particle size, and the composition of the leach solution.

This work is primarily focused on unraveling the dependency of these variables and their effects on the chalcopyrite dissolution rate by systematically analyzing each one in turn. In this analysis, it was assumed that mass transfer limitations are negligible given the large times for particle dissolution due to the slow nature of the intrinsic kinetics observed for chalcopyrite (Bouffard et al., 2006). With a view to developing a rigorous kinetic model for chalcopyrite leaching, the effect of particle size distribution must also be addressed. The overall mineral conversion is estimated for a distribution of particle sizes thus:

$$1 - \overline{X} = \int_{D_1}^{D_2} \left[1 - X(D,t)\right] f(D)\, dD \tag{3.2}$$

where *f*(*D*) represents the particle size distribution (PSD) in the form of a probability density function, and D_1 and D_2 are the particle sizes within which the PSD is delimited.

When the heterogeneous chemical reaction is the rate-limiting step, Equation 3.2 takes the following form:

$$1 - \overline{X} = \int_{D_1}^{D_2} \left(1 - \frac{t}{\tau(D)}\right)^3 f(D)\, dD \tag{3.3}$$

The PSD function must be determined for each mineral sample under study. Several practical forms of PSD are reported in the literature (Dixon and Dreisinger, 2003) and the acquisition of a particular one depends on the classification results of the material to

be used for the leaching tests. The process to determine the PSD parameters for a given mineral sample will be explained later on.

3.2 Modeling Anodic and Cathodic Polarization

Electrochemical theory can be useful in the development of a kinetic expression to be incorporated into the timescale as a function of the factors mentioned above. Dissolution kinetics of mineral sulfides (electron conductors) can often be described with the concepts of electrode kinetics. The Butler-Volmer equation in particular is used for the mathematical interpretation of potential-current density (*E*-*J*) relationships in the anodic and cathodic behavior of minerals. In this equation, electrochemical half-cell reactions occurring simultaneously are considered and studied as separate processes. These constitute the cathodic reduction of the oxidant, which in this particular case is the reduction of ferric to ferrous on the chalcopyrite mineral surface:

$$Fe^{3+} + e^{-} \rightarrow Fe^{2+} \tag{3.4}$$

and the consequent anodic oxidation of chalcopyrite:

$$CuFeS_2 \rightarrow Cu^{2+} + 2\,S^0 + Fe^{2+} + 4\,e^{-} \tag{3.5}$$

The kinetics of each process are modeled using the Butler-Volmer equation:

$$j = j_0\left[\exp\left(\frac{\alpha F\eta}{RT}\right) - \exp\left(\frac{-(1-\alpha)F\eta}{RT}\right)\right] \tag{3.6}$$

where j is the net current density, j_0 is the exchange current density (i.e., the current density of either half-cell reaction at the reversible potential), α is the transfer coefficient, F is Faraday's constant (96485 J/mol e^{-}), R is the universal gas constant (8.3143 J/mol/K), T is absolute temperature, and η is the overpotential:

$$\eta = E - E_R$$

where E_R is the reversible potential of the half-cell reaction.

Details of the derivation of this relationship can be found elsewhere (Bard and Faulkner, 2001). Equation 3.6 can sometimes be simplified depending on the magnitude of the

overpotential. An important criterion known as the “high field approximation” leads to simplified *E-J* relationships called Tafel equations:

For anodic processes where $\eta >> 0$:

$$j = j_0 \exp\left(\frac{\alpha F \eta}{RT}\right) \tag{3.7}$$

For cathodic processes where $\eta << 0$:

$$j = -j_0 \exp\left(\frac{-(1-\alpha) F \eta}{RT}\right) \tag{3.8}$$

The exchange current density j_0 depends on the particular kinetics of an electrochemical system and the rate constants associated with each half-cell reaction (e.g., Equations 3.4 and 3.5) are concealed in this value and must be estimated from the results of electrochemical experiments.

3.3 Mixed Potential Theory

The concept of mixed potential in electrochemistry can be applied to the modeling of several hydrometallurgical processes thus providing a valuable tool in the determination of process kinetics. According to the theory, half-cell reactions in an electrochemical environment occur simultaneously on charged surfaces until a dynamic equilibrium state is attained at a common mixed potential. The corresponding current density can be correlated with the rate of leaching through Faraday’s law.

Li et al. (1992) explained how the overall kinetics of these processes can be determined from analyzing the separate anodic and cathodic kinetics and obtaining a resulting mixed potential. However, limitations of methodology must be considered when complex systems such as chalcopyrite leaching are modeled. In order to illustrate some aspects of this theory, let us consider the reversible oxidation of a metal M by ferric, involving the interchange of two electrons:

$$M^0 = M^{2+} + 2\,e^- \tag{3.9}$$

$$2\,Fe^{3+} + 2\,e^- = 2\,Fe^{2+} \tag{3.10}$$

The expanded *E-J* relationship for each one is given as:

$$j^{ox} = j_a^{ox} + j_c^{ox} = z_a F\left[k_a^{ox} \exp\left(\frac{\alpha_a FE}{RT}\right) - k_c^{ox} C_{M^{2+}}^{s} \exp\left(\frac{-(1-\alpha_a)FE}{RT}\right)\right] \tag{3.11}$$

$$j^{red} = j_a^{red} + j_c^{red} = z_c F\left[k_a^{red} C_{Fe^{2+}}^{s} \exp\left(\frac{\alpha_c FE}{RT}\right) - k_c^{red} C_{Fe^{3+}}^{s} \exp\left(\frac{-(1-\alpha_c)FE}{RT}\right)\right] \tag{3.12}$$

where the subscripts *a* and *c* denote the anodic and cathodic branches of each reversible process, respectively, the superscripts *ox* and *red* denote the metal oxidation and ferric reduction half-cell reactions, respectively, and molar concentration at the metal surface is denoted by C^s.

The net current density is:

$$j = j^{ox} + j^{red} \tag{3.13}$$

As equilibrium is attained, this net current density becomes zero and the dissolution current takes the form of:

$$j_d = j^{ox}(E_m) = -j^{red}(E_m) \tag{3.14}$$

where E_m is the mixed potential.

The incorporation of an explicit kinetic expression based on electrochemical principles into the timescale is desirable for practical purposes. However, the use of the entire Equations 3.11 and 3.12 to find the mixed potential would involve solving a non-linear system of equations. Moreover, in the case of chalcopyrite, adsorption mechanisms influencing the electron transfer process may also be a function of this potential, as discussed later. Simplifications leading to expressions for the explicit mixed potential and the corresponding dissolution current density facilitate the derivation of an analytical rate expression. The estimation of the relative orders of magnitude for anodic and cathodic overpotentials from real kinetic experiments helps in the determination of assumptions to simplify expressions 3.11 and 3.12. Once the current densities evaluated at the mixed potential have been found, either the cathodic or the anodic rate expression can represent the overall leaching kinetics of mineral dissolution, and

dissolution current density may be converted into a molar dissolution rate with Faraday's law:

$$r = \frac{A_a j_d}{z_a F} = \frac{A_a j^{ox}(E_m)}{z_a F} \tag{3.15}$$

where A_a is the active surface area for anodic oxidation and z_a is the number of electrons transferred per mole.

Equations based on electrochemical principles may require additional modification in order to account for passivity in chalcopyrite leaching. It was assumed in this work that the electron transfer process is affected by adsorption of precipitates resulting from chemical speciation in the leaching solution, and that the solution potential determined by the ferric-to-ferrous ratio plays an important role influencing this mechanism. Thus, solution thermodynamics establish the conditions for adsorption and subsequent passivity to take place. From this perspective, the development of a chemical speciation model becomes necessary.

3.4 Speciation Modeling

During the last few decades there has been intensive effort to predict the redox potential in sulfate leach solutions as a function of the initial amounts of iron and copper, acidity, and temperature (e.g., Dry et al., 1988; Stripp et al., 1990; Casas et al., 2005). Unfortunately, speciation models developed in the past were poorly able to predict experimental values observed for potentials from various solutions used in the present work. In order to fill the empty gap of this practical necessity, a theoretical thermodynamic speciation model the H_2SO_4-$FeSO_4$-$Fe_2(SO_4)_3$-H_2O system was developed to determine the behavior of all species affecting passivity and to predict the solution potential as a function of temperature and the concentrations of acid and iron. Many discrepancies have been reported in the literature among authors regarding which complexes should be included in the speciation model for the H_2SO_4-$FeSO_4$-$Fe_2(SO_4)_3$-H_2O system to provide the best results. The criterion for selecting or rejecting different species in this model was based on the model's predictability of experimental results. The most important species reported in previous studies on the thermodynamics of this system were considered. The model developed here provides a mathematical tool

capable of quantifying the concentration of five free ions and eight complexes as functions of temperature, acidity level, and ferric-to-ferrous ratio. Table 3.1 shows these species with their relevant thermodynamic parameters and pertinent references. This set was found to be the best to predict accurately the experimental results. In subsequent sections, results of this thermodynamic model will help in the interpretation of passivity in the mathematical model of chalcopyrite.

Table 3.1 Complexes and their relevant thermodynamic parameters.

Species		log K_j (ref)	log K_j (app)	ΔH_f (cal/mol)	T range (^oC)
HSO_4^-	(E1)	1.99 [S]	1.99	$98T - 29{,}200$ [A]	–
$FeSO_4^0$	(E2)	2.20 [S]	2.20	1,560 [S]	22 – 90 [S]
$FeHSO_4^+$	(E3)	1.08 [S]	3.07	14,544 [D]	22 – 90 [D]
$FeSO_4^+$	(E4)	4.04 [C]	4.04	$272.73T - 78{,}033$ [C]	25 – 80 [C]
$Fe(SO_4)_2^-$	(E5)	5.38 [S]	5.38	–	–
$FeHSO_4^{2+}$	(E6)	2.48 [S]	4.47	15,216 [D]	22 – 90 [D]
$FeH(SO_4)_2^0$	(E7)	8.10 [C]	8.10	–	–
$CuSO_4^0$	(E8)	2.79 [R]	2.79	–	25 – 80 [R]

References: [A] Arslan, 2003; [C] Casas et al., 2005; [D] Dry et al., 1988; [R] Roine, 2002; [S] Stipp et al., 1990; [E] Estimated.

Eight chemical equilibria between the species are defined as follows:

$$H^+ + SO_4^{2-} \leftrightarrow HSO_4^- \quad \text{(E1)}$$

$$Fe^{2+} + SO_4^{2-} \leftrightarrow FeSO_4^0 \quad \text{(E2)}$$

$$Fe^{2+} + HSO_4^{2-} \leftrightarrow FeHSO_4^+ \quad \text{(E3)}$$

$$Fe^{3+} + SO_4^{2-} \leftrightarrow FeSO_4^+ \quad \text{(E4)}$$

$$Fe^{3+} + 2\,SO_4^{2-} \leftrightarrow Fe(SO_4)_2^- \quad \text{(E5)}$$

$$Fe^{3+} + HSO_4^{2-} \leftrightarrow FeHSO_4^{2+} \quad \text{(E6)}$$

$$Fe^{3+} + H^+ + 2\,SO_4^{2-} \leftrightarrow FeH(SO_4)_2^0 \quad \text{(E7)}$$

$$Cu^{2+} + SO_4^{2-} \leftrightarrow CuSO_4^0 \quad \text{(E8)}$$

Each of these equilibria has an equilibrium constant defined thus:

$$\log K_j = \sum_i v_{i,j} \log a_i = \sum_i v_{i,j} \log(\gamma_i C_i) \quad (3.16)$$

where $v_{i,j}$ is the stoichiometric coefficient of species i in equilibrium j, a_i is the activity of species i, γ_i is the activity coefficient of species i, and C_i is the molal concentration of species i.

Five component balances can be written in terms of the thirteen species as follows:

$$C_{\mathrm{H}} = C_{\mathrm{H^+}} + C_{\mathrm{HSO_4^-}} + C_{\mathrm{FeHSO_4^+}} + C_{\mathrm{FeHSO_4^{2+}}} + C_{\mathrm{FeH(SO_4)_2^0}} \tag{3.17a}$$

$$C_{\mathrm{Fe(II)}} = C_{\mathrm{Fe^{2+}}} + C_{\mathrm{FeSO_4^0}} + C_{\mathrm{FeHSO_4^+}} \tag{3.17b}$$

$$C_{\mathrm{Fe(III)}} = C_{\mathrm{Fe^{3+}}} + C_{\mathrm{FeSO_4^+}} + C_{\mathrm{Fe(SO_4)_2^-}} + C_{\mathrm{FeHSO_4^{2+}}} + C_{\mathrm{FeH(SO_4)_2^0}} \tag{3.17c}$$

$$C_{\mathrm{Cu}} = C_{\mathrm{Cu^{2+}}} + C_{\mathrm{CuSO_4^0}} \tag{3.17d}$$

$$\begin{aligned} C_{\mathrm{SO_4}} = {} & C_{\mathrm{SO_4^{2-}}} + C_{\mathrm{HSO_4^-}} + C_{\mathrm{FeSO_4^0}} + C_{\mathrm{FeHSO_4^+}} + C_{\mathrm{FeSO_4^+}} \\ & + 2C_{\mathrm{Fe(SO_4)_2^-}} + C_{\mathrm{FeHSO_4^{2+}}} + 2C_{\mathrm{FeH(SO_4)_2^0}} + C_{\mathrm{CuSO_4^0}} \end{aligned} \tag{3.17e}$$

The effect of temperature is estimated based on the van't Hoff equation:

$$\frac{\partial \log K_j(T)}{\partial T} = \frac{\Delta H_j(T)}{2.303\, RT^2} \tag{3.18}$$

where ΔH_j is the enthalpy change of reaction j, estimated from thermodynamic data reported in the work of other researchers (Dry and Bryson, 1988; Casas et al., 2005; Stripp, 1990). Finally, the redox potential of solution was calculated using the well-known Nernst equation, based only on the concentrations of free ferric and ferrous ions:

$$E = E^O + \frac{RT}{F} \ln \frac{C_{\mathrm{Fe^{3+}}}}{C_{\mathrm{Fe^{2+}}}} \tag{3.19}$$

where E^{O} is the standard potential for the Fe^{3+}/Fe^{2+} couple (0.771 V (SHE) at 25°C), which has the following dependence on temperature (Dry and Bryson, 1988):

$$\frac{dE^{\mathrm{O}}}{dT} = 1.19 \text{ mV K}^{-1} \tag{3.20}$$

The resulting set of non-linear equations was solved using the Newton-Raphson technique (Smith et al., 1970). In order to calculate solution potential, the model was solved for the concentration of free ferric and ferrous ions and the Nernst equation was

invoked. Initially, log K_j values reported in the literature were used. However, slightly different values were required to obtain the best fit of experimental data. The values of K_j reported in the literature are denoted “ref” in Table 3.1 and the estimated values used in the model are denoted “app” and are thought of as being apparent values where activity factors are implicitly incorporated. As a brief example, the apparent equilibrium constant for reaction (E3) would be conveniently defined as:

$$K_{\mathrm{E3}}^{app} = \frac{\gamma_{\mathrm{Fe^{2+}}}\gamma_{\mathrm{HSO_4^{2-}}}}{\gamma_{\mathrm{FeHSO_4^{+}}}} K_{\mathrm{E3}}^{ref} \tag{3.21}$$

This approach has been justified by Liddell and Bautista (1981), who used values of apparent equilibrium constants at typical ionic strengths found in leach liquors. This thermodynamic model provides an essential mathematical tool to predict the redox potential of the solution and also assists in modeling chalcopyrite passivity, as discussed in further sections.

CHAPTER 4 EXPERIMENTAL TECHNIQUES

In this chapter the experimental work required to elucidate the electrochemical and chemical behavior of chalcopyrite is described. The methodology adopted to obtain the desired experimental data from leaching tests of chalcopyrite under different oxidant concentrations is also examined.

4.1 Polarization Studies on Chalcopyrite Electrodes

4.1.1 Anodic polarization tests

A complete polarization study of the anodic breakdown of chalcopyrite, using electrodes fashioned from natural massive chalcopyrite samples from Chihuahua, Mexico, was undertaken by our research group (Viramontes-Gamboa et al., 2007). This study involved the generation and analysis of potentiostatic responses obtained at acidities from 2 to 100 g/L H_2SO_4 and temperatures from 25 to 80°C, with no added ferric or ferrous salts. Basically, the experiments consisted of applying external potentials at a scanning rate of 10 mV h^{-1} and measuring the steady-state current density response. Results from this work allowed the identification of the active (characterized by Tafel behavior), passive and transpassive potential regions. In the present work, kinetic parameters used for modeling the anodic behavior at 80°C and 70 g/L H_2SO_4 were extracted from the work just described.

4.1.2 Cathodic polarization tests

Estimation of dissolution current density using mixed potential theory requires a complementary analysis of cathodic behavior. Cathodic polarization tests to study the reduction of ferric on both fresh and pre-passivated chalcopyrite surfaces were conducted using a potensiostat (PARSTAT 2273, Princeton Applied Research) and a three-electrode cell. A saturated calomel electrode (SCE) was used as the reference electrode, a platinum wire as the counter electrode, and a massive sample of chalcopyrite cut into a cubic shape with a volume of approximately 0.8 cm^3 and mounted in epoxy resin was used as the working electrode. The mineral surface area exposed to solution was measured as 0.6 cm^2, and all current densities were based on this area. 700 mL of a solution containing H_2SO_4 (98%) and varying amounts of iron

salts added as $Fe_2(SO_4)_3(H_2O)_7$ and $FeSO_4(H_2O)_5$ was maintained at 80°C, stirred and purged with pure nitrogen gas previous to every cathodic scan. In this work, potentials are referenced and reported vs. the standard calomel electrode (SCE) for some electrochemical tests results, and the standard silver-silver chloride electrode (Ag/AgCl) for potentials in the leaching experiments.

4.2 Potential-Controlled Leaching Tests

Kinetic results from electrochemical experiments are contrasted with results from tank leaching tests to determine the level of applicability of mixed potential theory in this system. A series of potential-controlled leaching tests were conducted to obtain kinetic parameters embedded in the timescale from Equation 3.1 in order to characterize the chalcopyrite reaction rate and also to model extraction with the use of Equation 3.2. Leaching experiments were performed in 3 L sealed jacketed glass reactors with 1.5 L leaching solution containing sulfuric acid and iron sulfate salts. Temperature in all experiments was controlled at 80°C with a circulating hot water bath. Slurry samples of approximately 5 mL were taken at various times during the course of leaching and analyzed for copper with atomic absorption spectroscopy (AAS). In all tests, 20 g of massive chalcopyrite powder with a distribution of particle sizes ranging from 0.25 to 272.3 μm were used. Based on the results of quantitative XRD-Rietveld analysis, the sample consisted of 98.6% $CuFeS_2$ and 1.4% SiO_2, and the chemical content determined by inductively coupled plasma (ICP) revealed 28% total copper for the sample analyzed.

Good correlation between leaching rate and the corresponding solution potential can be attained if potential is properly controlled. Solution potential as an indicator of the oxidant concentration was controlled by setting a predetermined value in the controller for each leaching experiment and sparging pure oxygen gas into the slurry to regenerate ferric based on the following reaction:

$$4\ FeSO_4 + 2\ H_2SO_4 + O_2 \rightarrow 2\ Fe_2(SO_4)_3 + 2\ H_2O \qquad (4.1)$$

The slurry redox potential determined by the ferric-to-ferrous ratio in solution was measured with a redox probe (Ag/AgCl reference) which was connected to the controller. Solution potential values were also recorded at certain time intervals. Figure

4.1 shows the experimental setup used to control, measure and record experimental variables as solution potential and temperature.

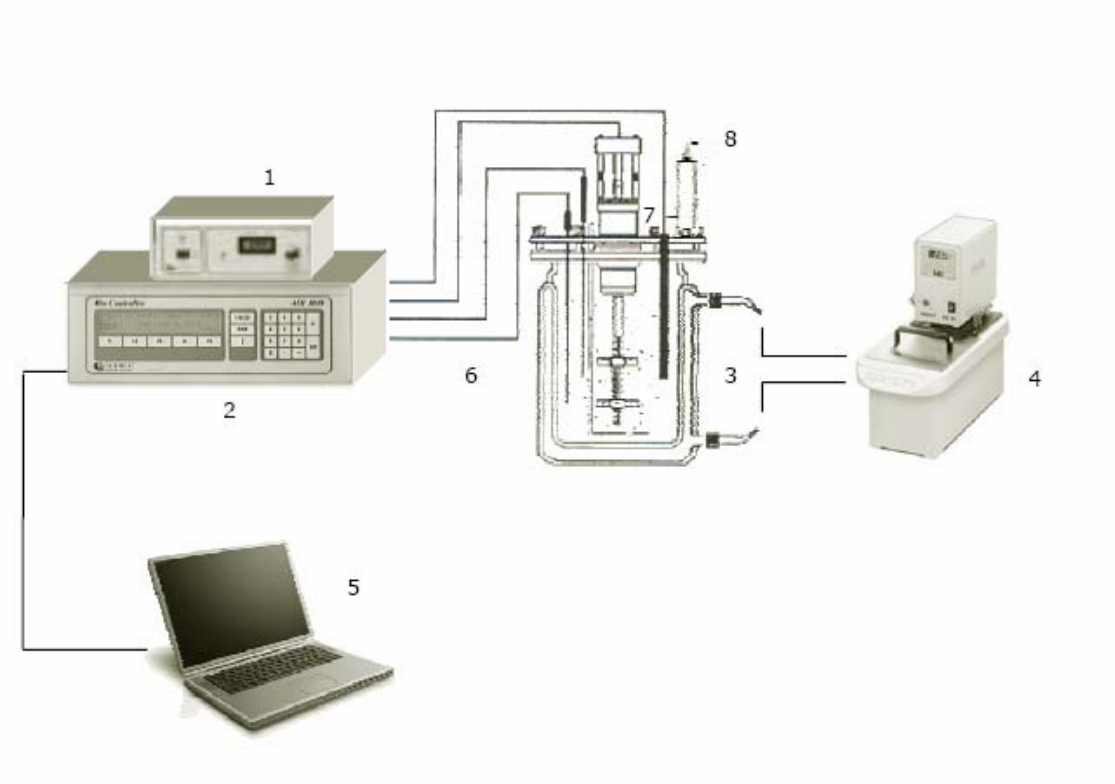

Figure 4.1 Experimental setup: (1) motor speed control, (2) bio-controller, (3) vessel, (4) water bath, (5) data acquisition, (6) redox probe, (7) agitator, (8) condenser.

4.3 Characterization of the Particle Size Distribution

Leaching is nearly always performed on a distribution of particle sizes rather than mono-sized particles. In order to represent the particle size distribution for the purpose of complete modeling, the chalcopyrite used in all tank leaching experiments was submitted to particle size distribution (PSD) analysis using a laser diffraction technique implemented by a Malvern Mastersizer 2000. The results are shown in Figure 4.2 in the form of a cumulative distribution in volume percent. These data were modeled using the Rosin-Rammler distribution function, which is commonly used to represent particle size

distribution data from milled samples. The mathematical form relating the probability density function to the particle size is given by:

$$f(\xi) = m\xi^{m-1}\exp(-\xi^m) \tag{4.2}$$

where $\xi = \frac{D}{D^*}$

and where D is diameter, D^* is reference diameter (which corresponds to the 63.21% mass passing size), and m is the Rosin-Rammler parameter.

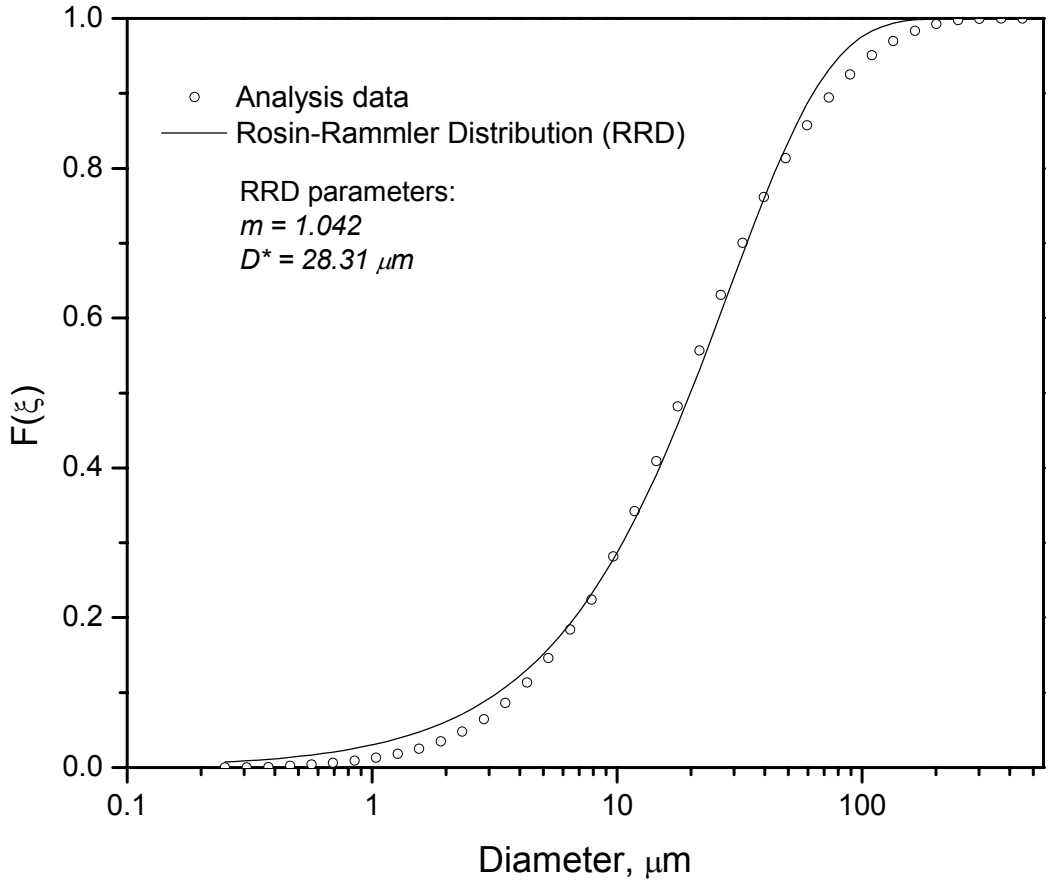

Figure 4.2 Cumulative distribution data and the best-fit Rosin-Rammler function.

CHAPTER 5 RESULTS AND DISCUSSION

In this chapter, the results from theory explained in Chapter 3 are presented and supported by experimental work. Firstly, the speciation model is validated and calibrated against measurements of solution potential for several conditions. This tool supports the hypothesis of passivity due to species precipitation and consequent adsorption on chalcopyrite surfaces as solution potential increases. The electrochemical aspects of chalcopyrite dissolution are also discussed. Anodic behavior accounting for passivity is modeled considering an adsorption mechanism of all ferric species promoting precipitation as a result of chemical speciation in the electrolyte.

Results from cathodic polarization studies performed on fresh and anodically pre-polarized chalcopyrite electrodes are discussed. As an ultimate conclusion, an expression for the dissolution of chalcopyrite based on electrochemical results is developed regarding the mixed potential as the reversible potential determined by the ferric-to-ferrous ratio.

5.1 Chemical Speciation

5.1.1 Redox potential data: experiment vs. theory

A comparison between the theoretical solution potential results from the speciation model and experimental measurements is shown in Figure 5.1. The open symbols indicate experimental values of redox potential in solution containing 25 g/L of total iron at 80°C, at various concentrations of sulfuric acid. The solid lines indicate the redox potential given by the theoretical model. The ferric-to-ferrous ratios indicated in the abscissa correspond to the initial values added as sulfate salts to the system.

5.1.2 Species concentration profiles

Figure 5.2 shows the concentration profile for all species considered in the model at 80°C, 25 g/L total Fe, and 70 g/L H_2SO_4. The same general trends observed for other conditions as those in the figures are maintained. It should be observed that several of these species show an increasing concentration tendency as solution potential increases, and $FeHSO_4^{2+}$, $FeH(SO_4)_2^{0}$ and $FeSO_4^{+}$ are particularly prevalent.

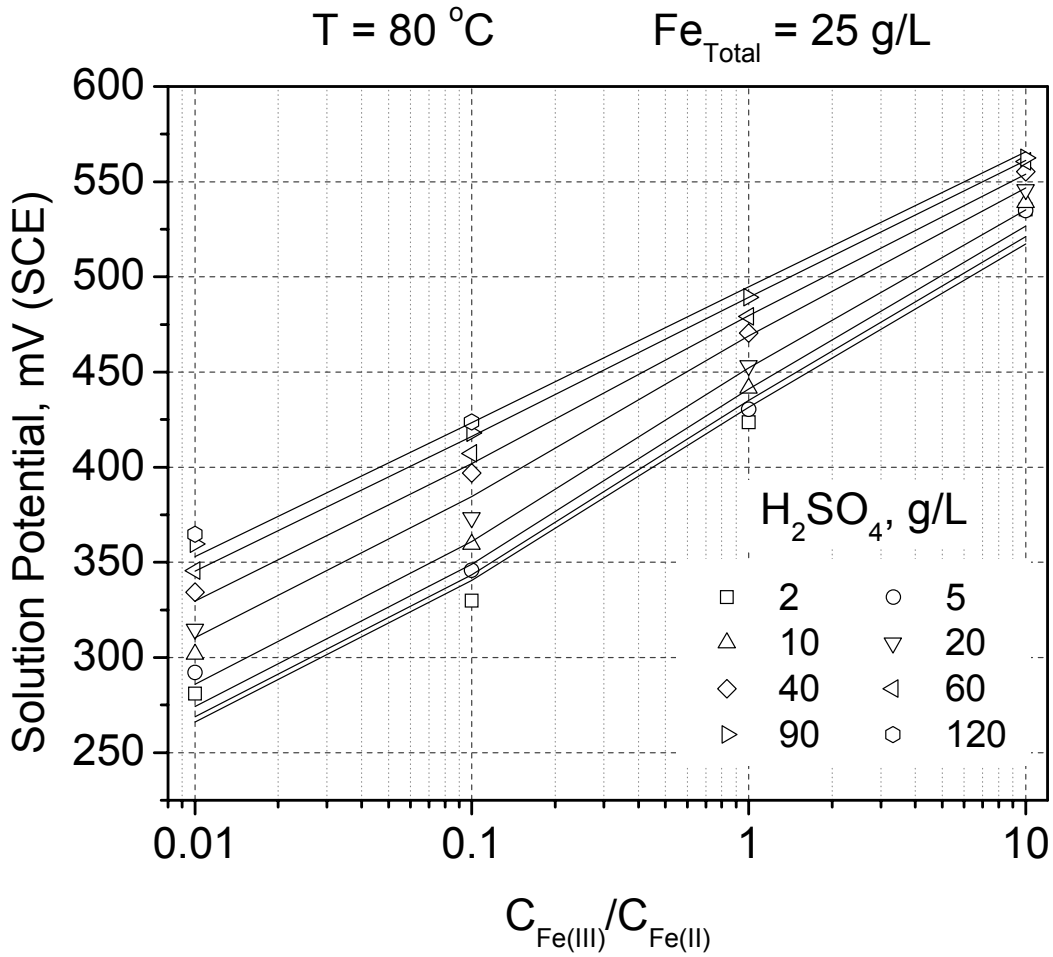

Figure 5.1 Experimental values of the redox potential (symbols) compared with the theoretical predictions of the model (solid lines).

This behavior supports the idea of ferric species promoting precipitation and adsorption on the chalcopyrite surface as it is polarized. During anodic polarization, positive charges become abundant on the mineral surface, thus positive species could either be slightly attached to the surface or be repelled by electrostatic forces. In principle, all ferric-containing species would interact with the chalcopyrite surface, although for purposes of simplicity and modeling, only the neutral species $FeH(SO_4)_2^0$ was considered as to be eligible for participating in the adsorption process since the functional relationship between all the other ferric complex ions and solution potential remains the same. Predictions of the kinetic model, as shown later, do not depend on the inherent chemical characteristics of the species believed to participate in passivity

but only on the functional form of concentration related to potential changes. Furthermore, the remarkable shape of the concentration curve suggests that a mechanism of adsorption can be envisaged without necessarily having to inquire in detail about the specific chemical interactions occurring at the mineral surface.

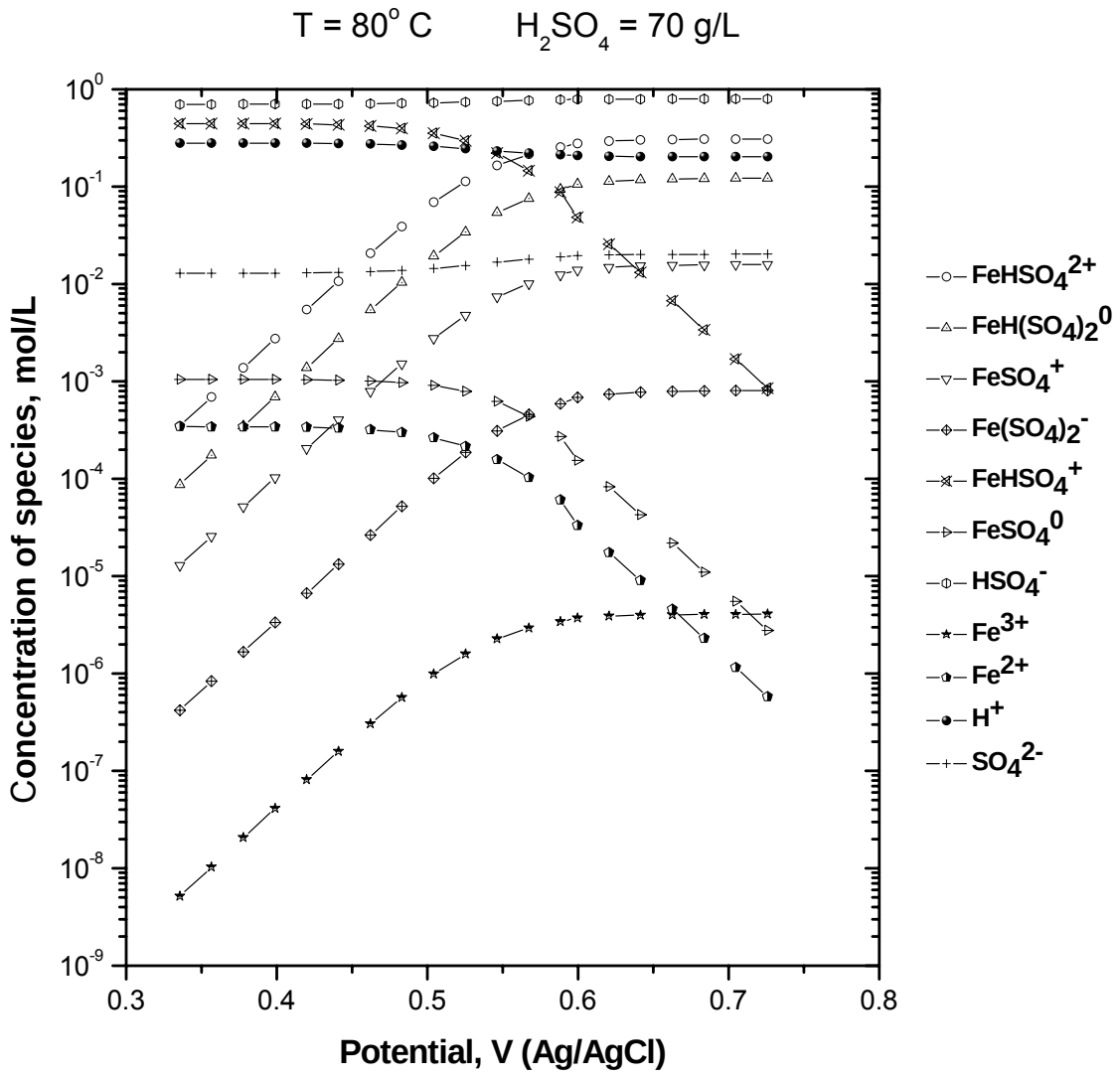

Figure 5.2 Concentration of all species predicted by the speciation model

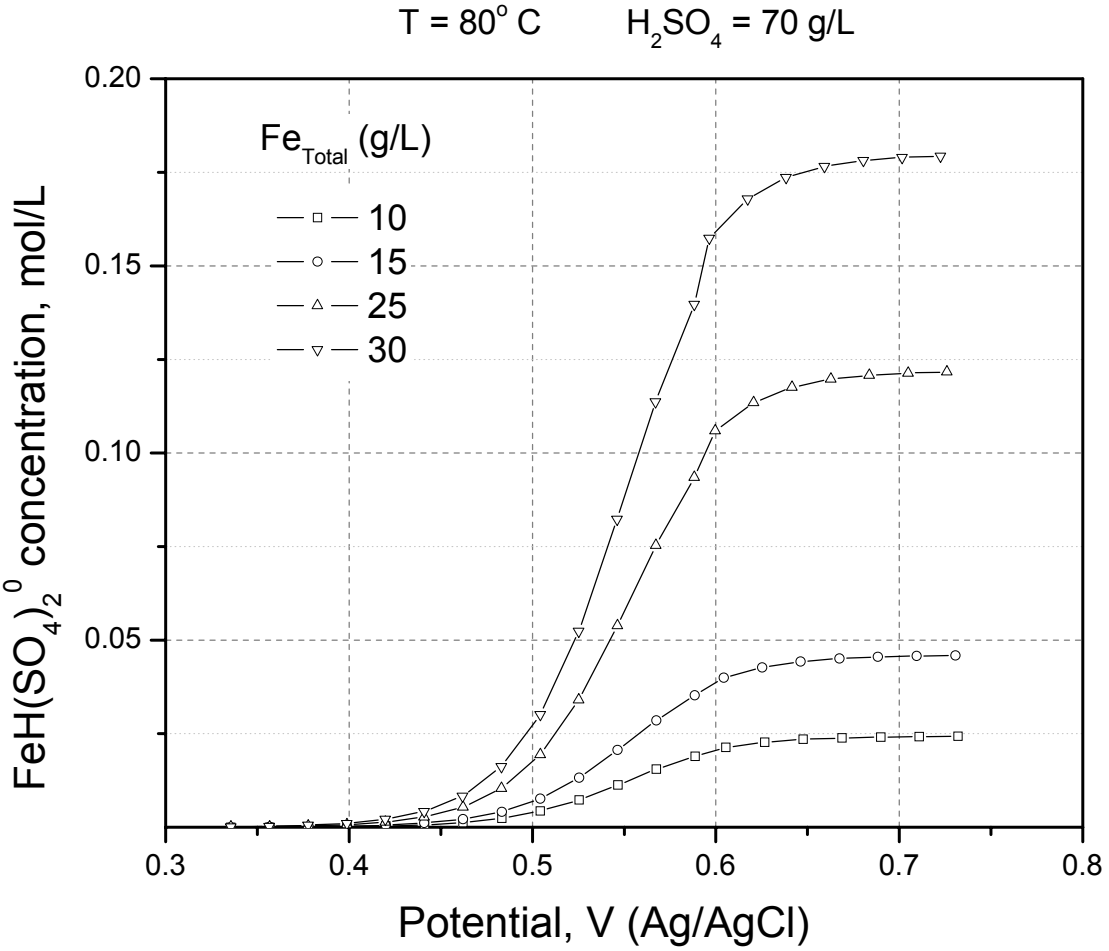

Figure 5.3 Influence of total iron concentration on the behavior of $FeH(SO_4)_2^0$ as solution potential increases.

5.1.3 Concentration of adsorbed ferric species vs. potential

The concentration-potential relationship used later in the model for the behavior of species interacting chemically to promote participation by an adsorption mechanism was modeled considering only the neutral complex $FeH(SO_4)_2^0$ using a sigmoidal function to fit the speciation results:

$$C = \frac{C_{max}}{1 + \exp\left[-a(E-b)\right]} \tag{5.1}$$

where C is the molar concentration of $FeH(SO_4)_2^0$, E is the solution potential, and C_{max}, a and b are fitting parameters for a particular set of conditions of temperature, total iron and acid concentration, which to be determined using the speciation model. Particularly, total iron concentration is important to consider when Equation 5.1 is used. Values for C_{max} vary considerably depending on the amounts of total iron dissolved as shown in Figure 5.3. Results from the speciation model and their corresponding representation using Equation 5.1 are shown in Figure 5.4.

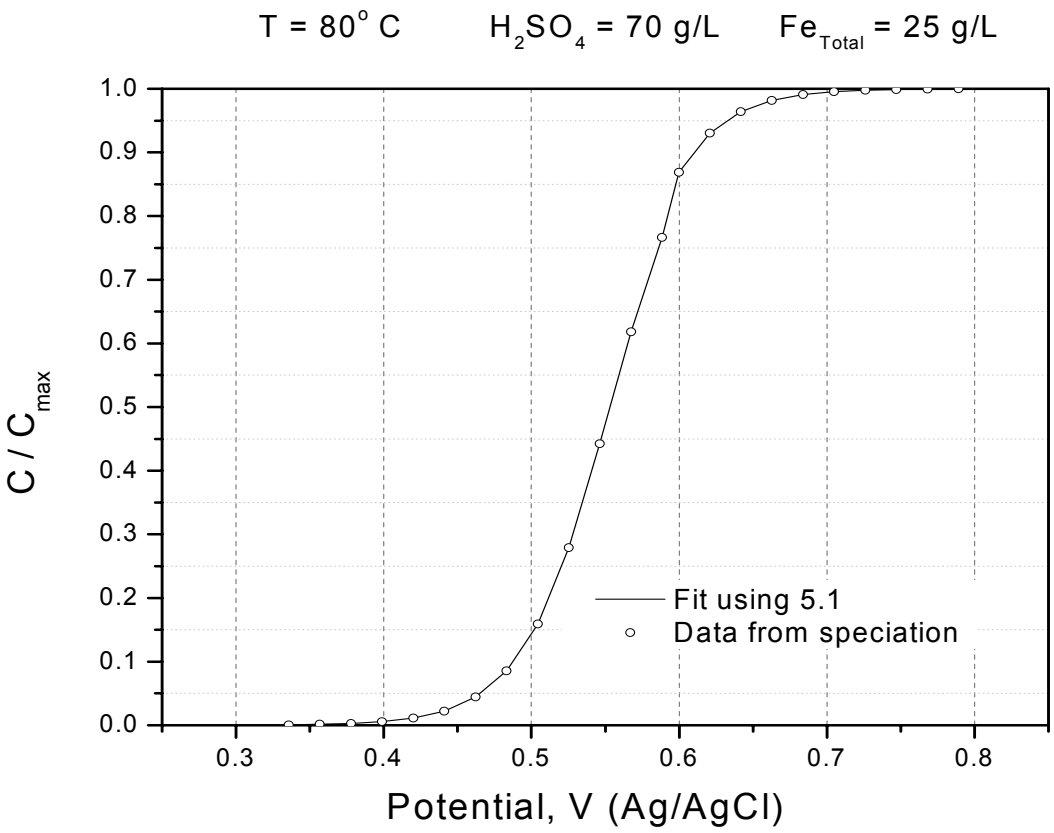

Figure 5.4 Description of $FeH(SO_4)_2^0$ concentration using Equation 5.1.

5.2 Electrochemical Analysis

The kinetic model derived from mixed potential considerations in this work is based on the characterization of cathodic and anodic polarization behavior of chalcopyrite. The electrochemical behavior for each half-cell reaction was quantitatively modeled and pertinent assumptions were made towards the derivation of a practical analytical expression for the reaction rate of chalcopyrite leaching.

5.2.1 Anodic behavior and its mathematical modelling

As long as the anodic mineral breakdown is considered an irreversible process and the anodic overvoltage is high, the *E*-*J* relationship for this anodic process can be simplified by neglecting the cathodic contribution as stated in Equation 3.7. In addition, passivity occurring on the surface at certain potentials diminishes the active anodic surface area thus hampering the electron transfer process. This passivity in the potentiostatic tests occurs as a result of applying an external potential on the surface thus allowing the partial conversion of ferrous to ferric in the Nernst layer. In accordance to previous results from the speciation model several ferric complexes may be responsible for causing passivity. Thus, a factor for the coverage of ferric-bearing species on the mineral surface is incorporated, signifying that the surface of the mineral is blocked by this passivating species, which is probably $FeH(SO_4)_2^0$. Taking into account these considerations, Equation 3.7 must be modified as:

$$j^{ox} = j_a^{ox} = z_a F\, k_a^{ox} (1-\theta) \exp\left(\frac{\alpha_a FE}{RT}\right) \tag{5.2}$$

where θ represents the fraction of the surface blocked. Thus, θ = 1 implies total surface blockage, while θ = 0 implies no blockage at all.

The surface blockage mechanism was modeled by Langmuir adsorption which represents the surface coverage as a function of the adsorbed species concentration (Duang, 1988). By Langmuir's theory the surface coverage in the absence of an electric field is given by:

$$\theta = \frac{bC^n}{1+bC^n} \tag{5.3}$$

where C is the molal concentration of the adsorbing species, n is an adsorption order factor accounting for the mechanism by which the adsorption sites interact with the adsorbing molecules, and b is a function of the activation energy for adsorption and desorption, E_a, thus:

$$b = b_0 \exp\left(\frac{E_a}{RT}\right) \tag{5.4}$$

Under the influence of strong electric fields, the adsorbed molecules develop dipolar, quadripolar, or superior polar structures, causing a strong interaction between the electric field and the molecules. In the simplest case, the molecules develop dipolar momenta with interaction energies proportional to the electric field. Under conditions of strong adsorption the field free activation energy E_a is modified, and a higher energy barrier must be surmounted in order to desorb the strongly attached molecules. If the mineral is polarized, either by the application of an external (electrochemical) field or by the presence of a redox couple, the energy barrier is increased by a factor proportional to the applied potential. The new value of b becomes:

$$b = b_0 \exp\left(\frac{E_a + \beta FE}{RT}\right) \tag{5.5}$$

where β is a parameter accounting for the strength of the interaction between the molecules and the surface under the influence of an applied potential E.

If the expression for θ is substituted into Equation 5.2, the new anodic current density becomes:

$$j^{ox} = z_a F \frac{k_a^{ox} \exp\left(\frac{\alpha_a FE}{RT}\right)}{1 + b_0 \exp\left(\frac{E_a + \beta FE}{RT}\right) C^n} \tag{5.6}$$

Electrochemical parameters for the anodic branches are estimated by fitting Equation 5.6 to experimental anodic polarization curves shown in Figure 5.5. At n = 1 the model fits the experimental data very well around the passivity potential E_{pp} (the onset potential where current density begins to decrease), but deviates at potentials in the

passive range. At n = 3 the model fits the passive region very well, but deviates around E_{pp}. For this reason the model fits the data much better when n is taken as a sigmoid function of potential between the values of 1 and 3:

$$n = 1 + \frac{2}{1 + \exp(n_1 E + n_2)} \tag{5.7}$$

One might speculate that the reason for this may be that at lower potential, the ferric species are adsorbing one by one onto individual adsorption sites, while at higher potential, they may be adsorbing three at a time into jarosite precipitates.

Also, although not strictly required, further improvement is obtained when the proportionality constant β is allowed to vary linearly with the potential, thus:

$$\beta = \beta_1 E + \beta_2 \tag{5.8}$$

These two improvements to the model reproduce the observed experimental anodic curve with passivity (see Figure 5.4) giving good fits to the experimental data for other conditions. The five fitting parameters shown in Table 5.1 were determined for the following experimental conditions: T = 80°C, 70 g/L H_2SO_4 and 25 g/L total iron.

Table 5.1 Kinetic parameters used in the anodic polarization model.

Passivity parameters		Tafel parameters		Speciation parameters	
b_0	2.99×10^{-11}	k_a^{ox}	8×10^{-17} mol cm^{-2} s^{-1}	C_{max}	0.122 M
n_1	0.0124	α_a	1	a	0.0355
n_2	–9.169			b	552.35
β_1	–0.0006				
β_2	1.556				
E_a	10 RT				

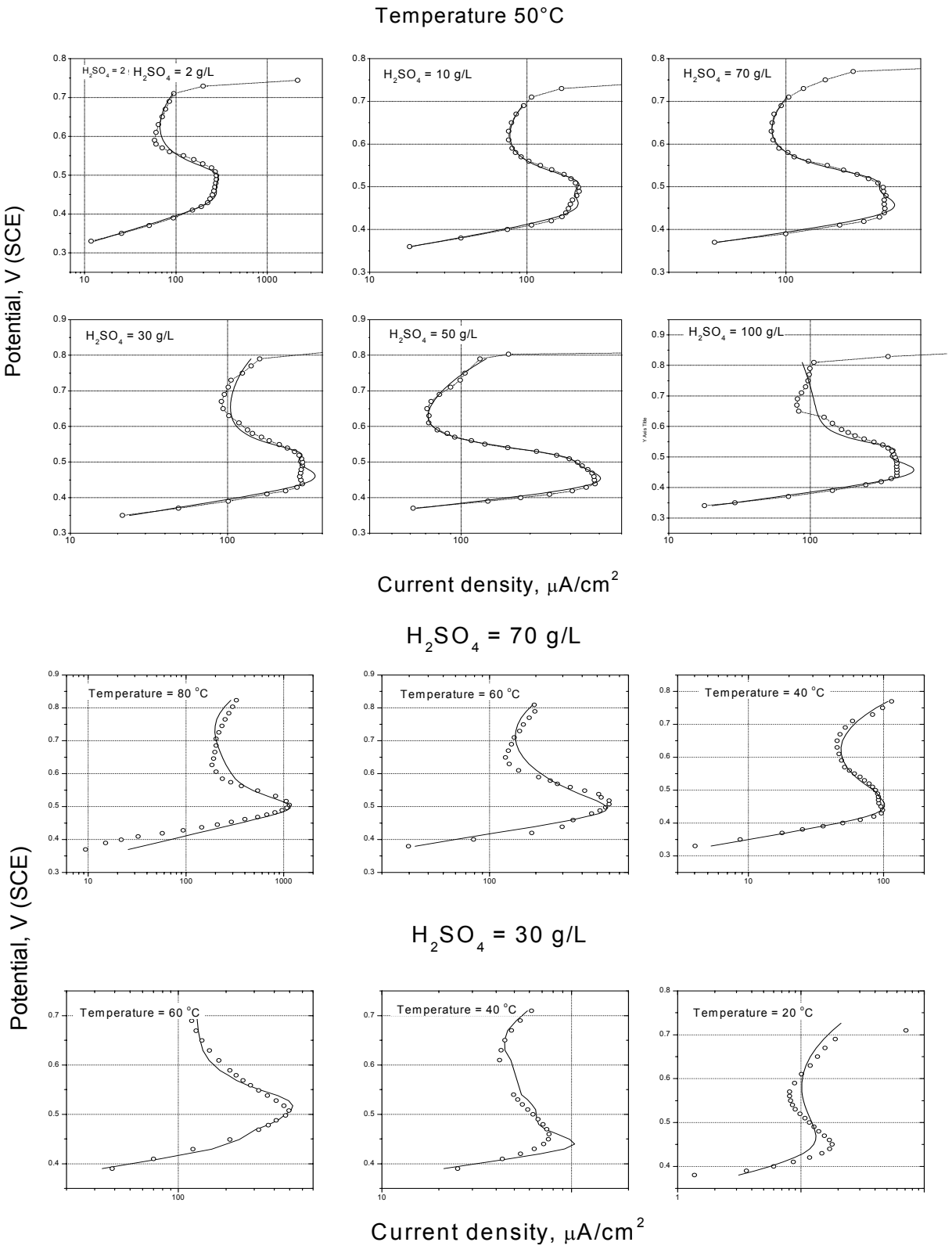

Figure 5.5 Anodic polarization curves for chalcopyrite at various temperatures and acid concentrations, and their mathematical representation including corrections for parameters *n* and *β*.

5.2.2 Cathodic behavior

Cathodic polarization curves were obtained using chalcopyrite electrodes to investigate the effect of variables such as total iron concentration, polarization scanning rate, and the ferric-to-ferrous ratio in solution. It can be observed from Figure 5.6 that current density becomes increasingly higher with increasing iron concentration. For purposes of determining the mixed potential, this observation has an important impact, since the effect of total iron concentration should be strictly considered if the anodic curve is located at high overpotential regions where divergence of current density is more pronounced.

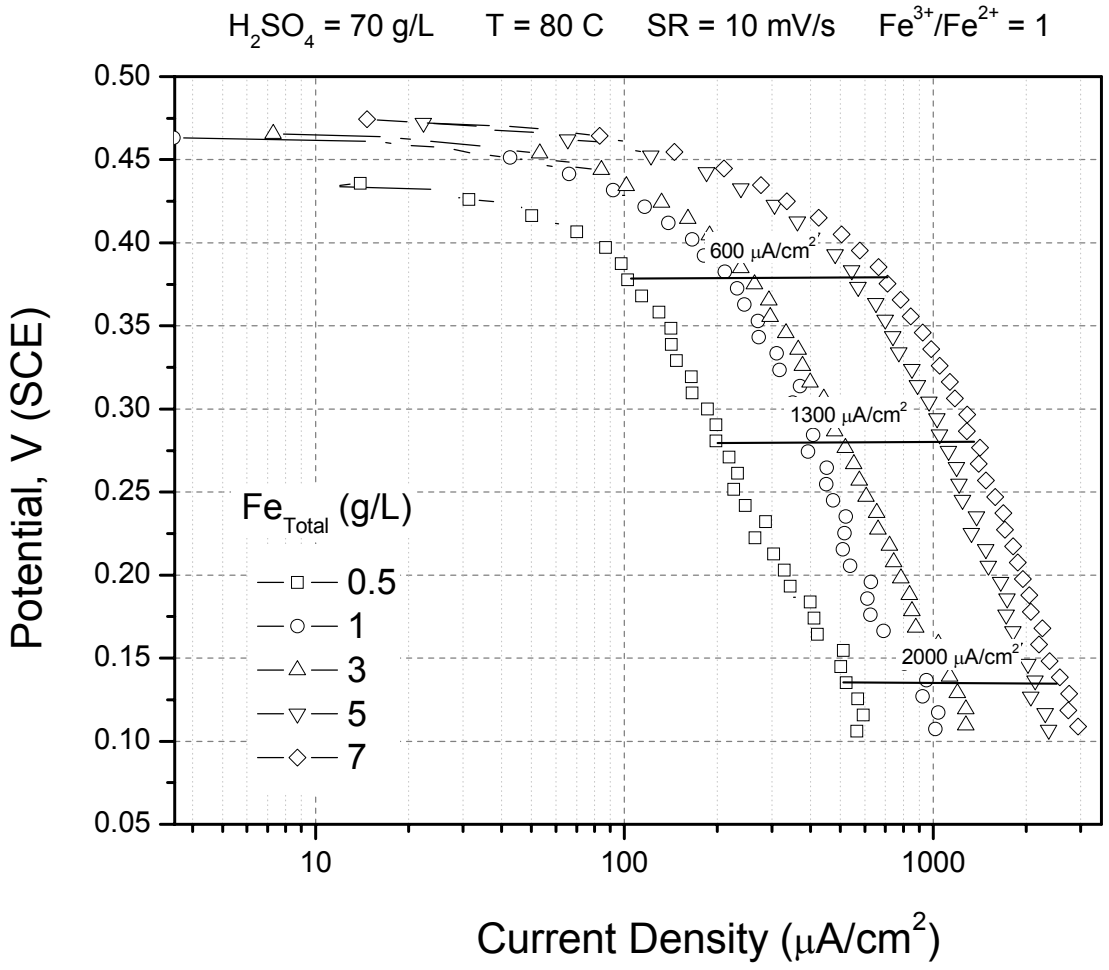

Figure 5.6 Cathodic polarization curves at various initial total iron concentrations.

Figure 5.7 shows that larger current densities are also obtained at higher polarization rates. As can be observed in Figures 5.6 and 5.7, the effects of total iron and scanning rate can be minor, as long as the mineral open-circuit potential (rest potential) is near to the range of the reversible potential determined by the ferric-to-ferrous ratio in the bulk solution, which varied approximately from 425 to 475 mV and was found to be independent of scanning rate (lying near 425 mV).

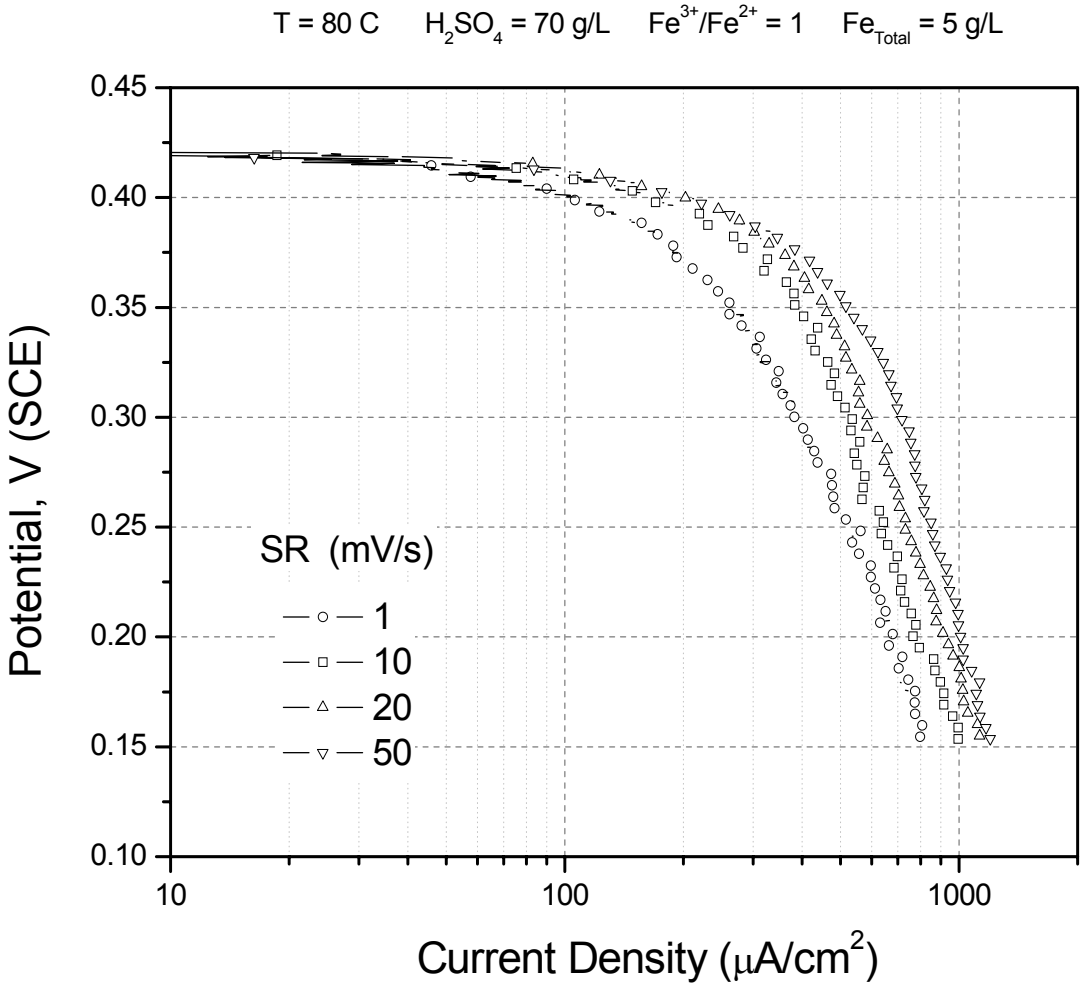

Figure 5.7 Cathodic polarization curves performed at different scanning rates.

The theoretical *E-J* relationship for the cathodic reaction based on the Butler-Volmer equation incorporates a proportional and direct dependence on the concentration of ferric and ferrous ions, depending on the reversibility of the ferric reduction reaction and the magnitude of the cathodic overpotential. Hence, ferric and ferrous concentrations are expected to influence significantly the cathodic polarization response and also the ferric-ferrous equilibrium potential determined by the Nernst equation and estimated with the aid of the speciation model. Figure 5.8 shows the effect of different ferric-to-ferrous ratios at fixed total iron and acid concentrations and scanning rate.

Characterization of mineral reduction by electrochemical techniques provides insight into the general cathodic behavior for the sample studied. However, in some cases, reaction rates determined from electrochemical studies using Evans diagrams are not comparable to reaction rates observed in a leaching environment where simultaneous exchange of electrons at grain level may take place differently as opposed to the electrode level in polarization tests (Luna-Sanchez et al., 2003). Moreover, passivity observed during anodic polarization might also influence the response of ferric reduction on chalcopyrite surfaces (Tshilombo et al., 2004).

In order to more closely simulate the leaching environment, the effect of ferric reduction on real passivated surfaces was investigated by performing cathodic polarization on anodically pre-passivated chalcopyrite surfaces. The anodic potentials applied for different tests were chosen to be representative of particular regions along the anodic curve. It is observed in Figure 5.9 that the open-circuit potentials at the beginning of each test dropped and converged to a similar value of approximately 0.38 V regardless of the applied potential intended (0.65 V for the passive region, 0.42 V for the active region, and 0.49 V for the onset of passivity). However this was not accomplished for the polarization test performed on a clean surface where there was an insignificant drop from 0.49 V (OCP) to 0.45 V, which might have been attributed to normal variations in the potential recorded by the potensiostat device. In this experiment, no ferrous ions were added initially, so ferrous oxidation did not contribute to the total current.

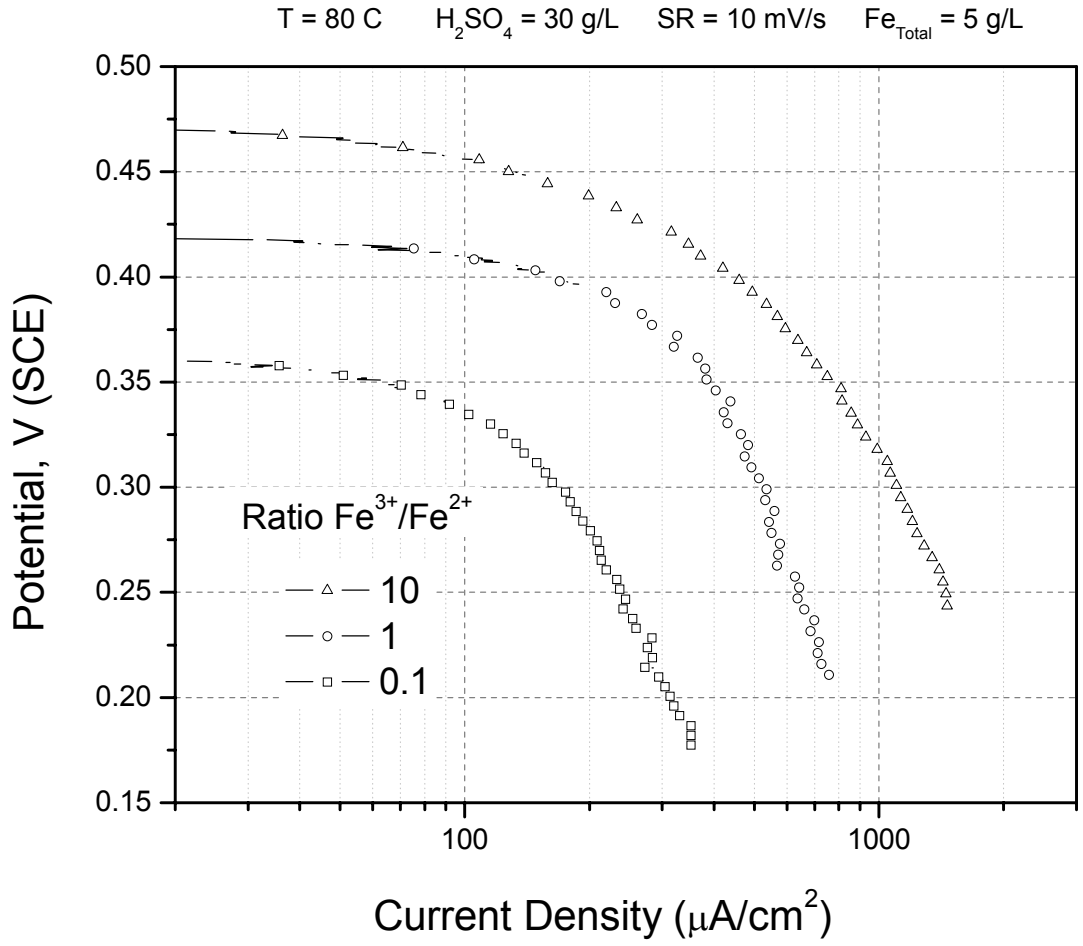

Figure 5.8 Ferric-to-ferrous ratio effect on the cathodic polarization.

5.3 Mixed Potential Theory to Explain Chalcopyrite Leaching Kinetics

Based on experimental results from the separate anodic and cathodic polarization tests, important conclusions can now be drawn:

1. The shape of the anodic polarization curve under various conditions of acid concentration and temperature are well modeled by considering the adsorption of ferric species and incorporating the coverage fraction as a function of redox potential.

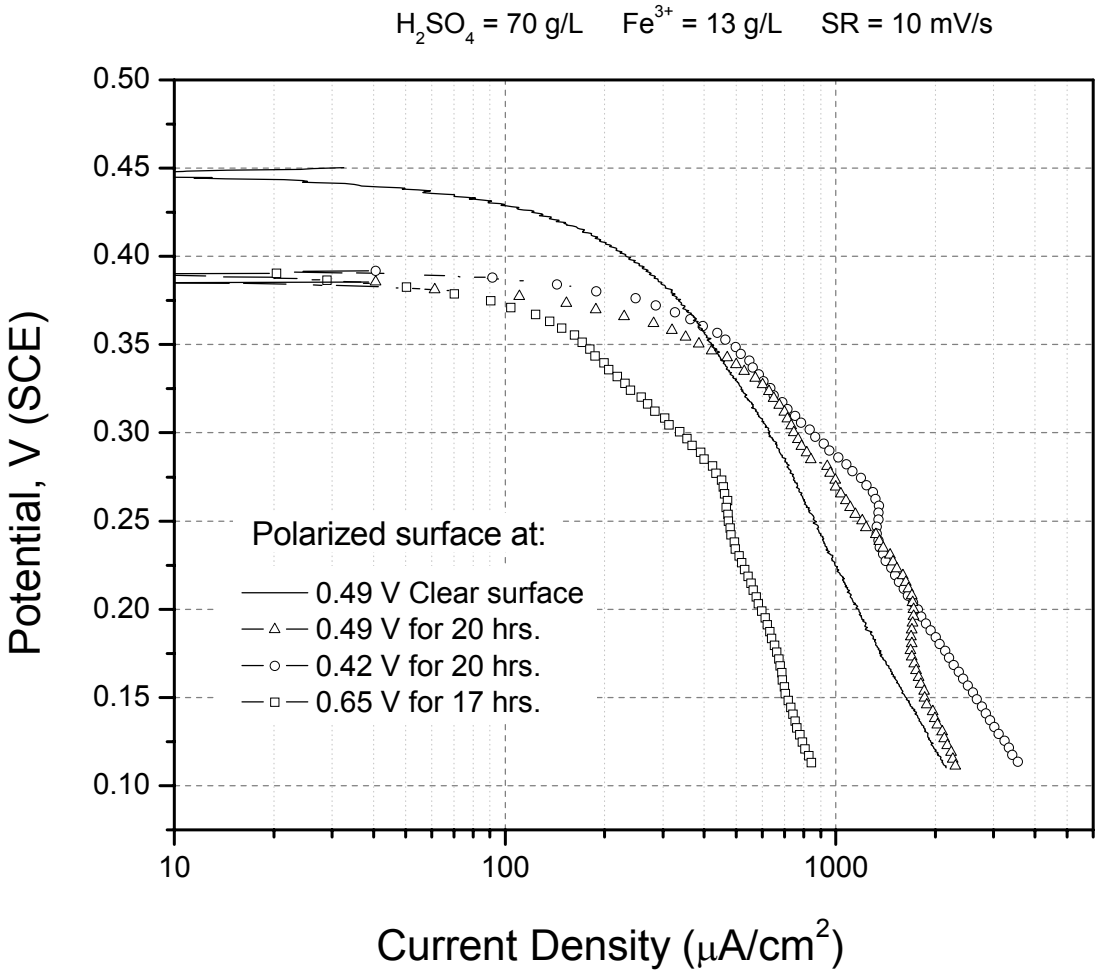

Figure 5.9 Polarization curves obtained from cathodic reduction on various pre-passivated surfaces.

2. The chemistry and thermodynamics of the solution determine the local concentrations of ferric and ferrous ions present in the solid-liquid interface and also the solution potential in the leach liquor, thus having a strong influence on the adsorption process attributed to species involved in passivation.

3. All polarization tests for the reduction of ferric ions on the chalcopyrite surface revealed that only a narrow region around the ferric-ferrous reversible potential needs to be considered in order to determine the mixed potential if the mineral rest potential lies around this region. As a result, there is no point in modeling the cathodic behavior at large cathodic overpotentials even when the scanning rate, total

iron concentration or other variables cause drastic variations in the cathodic current density. Therefore, the mixed potential will always be bounded within regions of cathodic low overvoltage, and the use of Nernst equation suffices to model the effects of ferric-to-ferrous ratio and calculation of the mixed potential.

In the cathodic branch, the reversible potential for the ferric-to-ferrous couple determines the mixed potential in the region of low overvoltage (see Figure 5.10):

$$E = E_R = E^{\circ} + \frac{RT}{F} \ln\left(\frac{C_{Fe^{3+}}}{C_{Fe^{2+}}}\right) \tag{5.9}$$

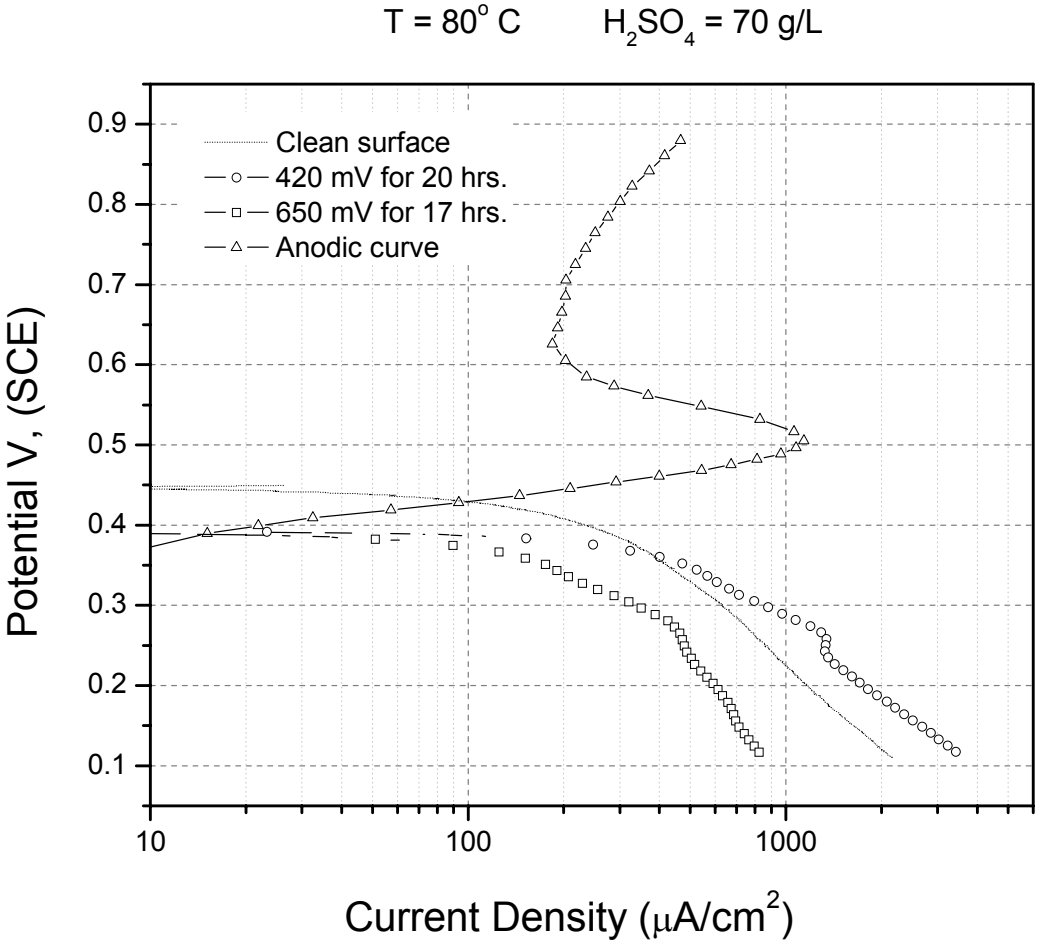

Figure 5.10 *E-J* plots showing regions where mixed potential can be determined.

Substituting Equation 5.9 into Equation 5.6 and invoking Faraday's Law gives:

$$J_d^{elec} = \frac{j^{ox}}{z_a F} = \frac{k_a^{ox} \exp\left(\frac{\alpha_a F E^{O}}{RT}\right)\left(\frac{C_{Fe^{3+}}}{C_{Fe^{2+}}}\right)^{\alpha_a}}{1 + b_0 \exp\left(\frac{E_a + \beta F E^{O}}{RT}\right)\left(\frac{C_{Fe^{3+}}}{C_{Fe^{2+}}}\right)^{\beta}} \tag{5.10}$$

where J_d^{elec} is the dissolution rate expressed in mol/s/cm^2 and the superscript "elec" means that this value is estimated from electrochemical experiments.

Simplyfing:

$$J_d^{elec} = \frac{k_a'\left(\frac{C_{Fe^{3+}}}{C_{Fe^{2+}}}\right)^{\alpha_a}}{1 + B\left(\frac{C_{Fe^{3+}}}{C_{Fe^{2+}}}\right)^{\beta} C^n} \tag{5.11}$$

where:

$$k_a' = k_a^{ox} \exp\left(\frac{\alpha_a F E^{O}}{RT}\right)$$

and:

$$B = b_0 \exp\left(\frac{E_a + \beta F E^{O}}{RT}\right)$$

Considering the assumptions discussed in section 3.1, the differential equation describing the fraction unreacted for a particle of diameter D_0 is related to the dissolution rate thus:

$$\frac{dX}{dt} = \frac{6M}{\rho D_0} J_d^{elec} (1 - X)^{\frac{2}{3}} = \frac{3(1 - X)^{\frac{2}{3}}}{\tau} \tag{5.12}$$

where ρ is the chalcopyrite mass density and M is chalcopyrite molecular weight, and the timescale is given thus:

$$\tau = \frac{\rho D_0}{2M} \frac{1 + B\left(\frac{C_{Fe^{3+}}}{C_{Fe^{2+}}}\right)^{\beta} C^n}{k'_a \left(\frac{C_{Fe^{3+}}}{C_{Fe^{2+}}}\right)^{\alpha_a}} \tag{5.13}$$

where C, n and B depend implicitly on the redox potential as well, as discussed above.

5.4 Mathematical Model of Chalcopyrite Reaction Rate

5.4.1 Experimental extraction curves

Several tank leaching experiments were performed to obtain extraction curves at various oxidant concentrations. In each experiment, there was an attempt to control the solution potential by adjusting the flow of oxygen gas necessary to convert the ferrous back to ferric in solution. The solution potential indicated at the top of the plots in Figure 5.11 was an intended average potential defined as that at which the leaching conditions were maintained the longest. It must be noticed that better potential control was attained for experiments with solution potentials in the active region, considered to be within the range of 415 to 470 mV (Ag/AgCl).

When leached under potentials within the active region, the chalcopyrite sample used in this study exhibited oxidation kinetics similar to other secondary sulfides such as chalcocite, where the influence of increasing amounts of ferric ions provide increasing levels of extraction (Bolorunduro, 1999). The best extraction performance in the active region was obtained for the test carried out at 470 mV and this was considered to coincide with the onset of passivity. This potential falls within the region of potentials identified by other researchers who have observed the onset of passivity (Kametani and Aoki, 1985; Pinches et al., 2001). Results from leaching tests carried out under potentials higher than 470 mV showed a drastic decrease in the dissolution rate. The experiment performed at 500 mV showed a slower rate of leaching than those tests conducted in the active region (see Figure 5.11e), although this test began at approximately 470 mV (within the passive region) but shifted to 500 mV after a couple

of hours, after which the surface was believed to be passivated and thereafter the chalcopyrite continued to leach at relatively lower rates.

5.4.2 Potential values for validation

Considering that the potentials at which chalcopyrite was leached fluctuated with time, it is important to identify these potentials for the purpose of validating the kinetic model and representing dissolution rates for each leaching test. This identification may not be totally clear when the leaching takes place in regions where the mineral surface is passivated, because the leaching rate is so sensitive to changing solution potential.

A direct comparison between two similar experiments helps illustrate this point. Figure 5.12 shows results from two leaching tests taking place at 490 and 500 mV. Even though the same trend for extraction levels is observed, solution potential evolved differently for each test. For the 490 mV test, solution potential started at approximately 490 mV, rose to 500 mV after about 5 hrs leaching, and then fell back to 490 mV without any noticeable improvement in the rate of copper extraction. In the experiment at 500 mV, on the other hand, solution potential rose very quickly to 500 mV and remained there during the first 20 hrs, and only afterwards increased to around 510 mV, coinciding with a possible decrease in leaching rate. These observations lead to a couple of possible alternatives for defining the potential to represent the corresponding dissolution rates:

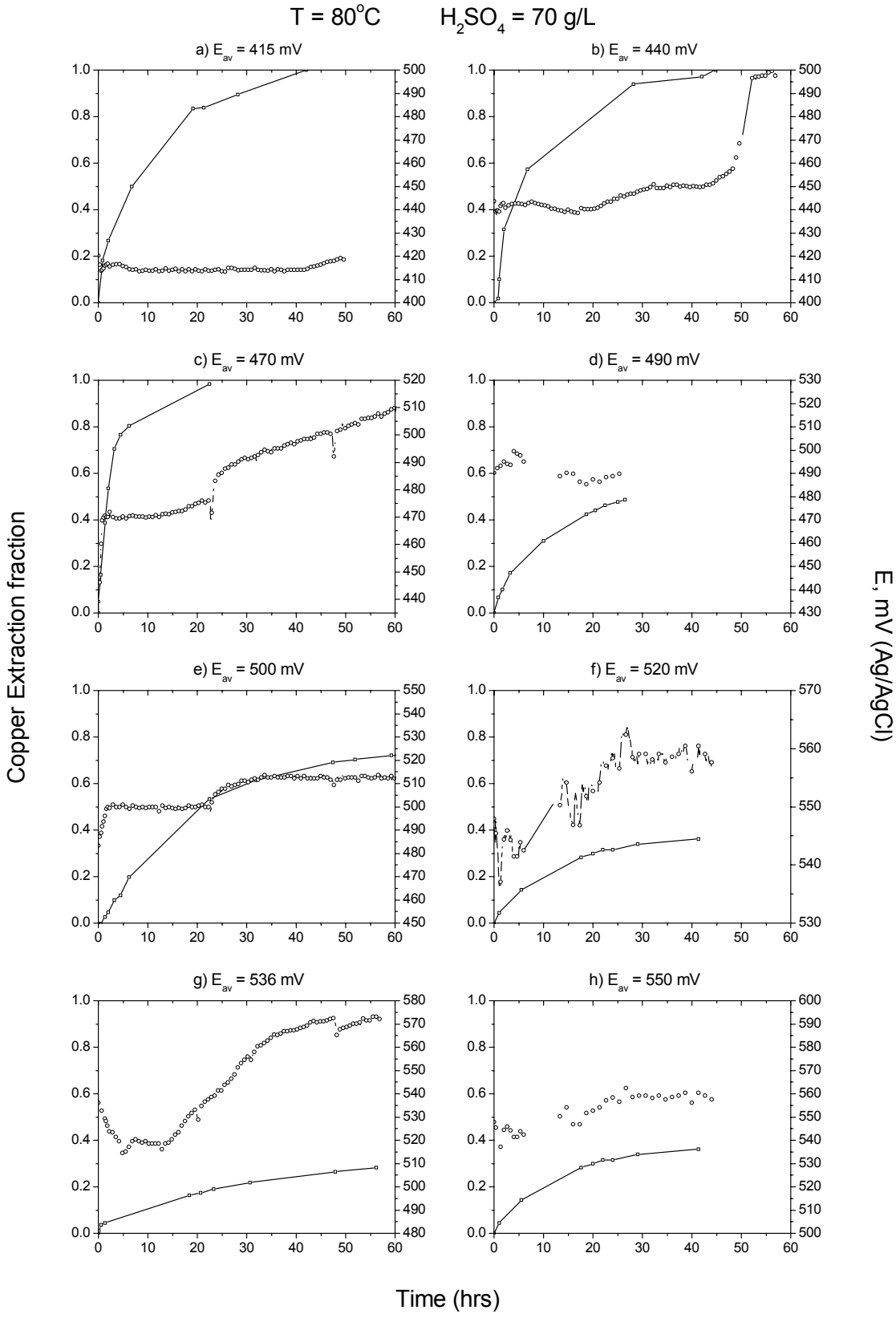

Figure 5.11 Copper extraction curves obtained at various solution potentials recorded during the course of leaching.

1. The starting solution potential

In kinetic studies, the reactant concentration representative of the leaching rate is almost always reported as the concentration determined by the initial distribution of species regardless of the redistribution of all participating species during the course of reaction. Instead, it would be desirable to maintain a constant concentration of oxidant species in order to obtain more reproducibility in the leaching rate predictions. However, due to passivity encountered in chalcopyrite, this convention of initial potential cannot be made, because, as observed in Figure 5.12, solution chemistry affects the mechanisms at the chalcopyrite surface rendering a situation where reaction rate can not be correlated with simply the initial oxidant concentration.

2. The highest passive potential reached

Chalcopyrite passivity beginning at a determined redox potential, as discussed above, is the result of interaction between species in solution and at the mineral surface by means of adsorption and precipitation. In this study these mechanisms were believed to take place irreversibly in a way that leaching rate did not change once the leaching solution had reached the first highest potential. This observation contrasts that made by Dixon and Petersen (2002) who found that a sudden increase of solution potential in heap leaching did not change the rate of copper extraction, possibly due to the short duration of the high potential episode in their experiment (on the order of days).

For validation purposes, potentials representing the leaching rates in this study were taken as those average values for well-controlled tests, and the first highest potential observed in the potential evolution curve was used when passivity was observed.

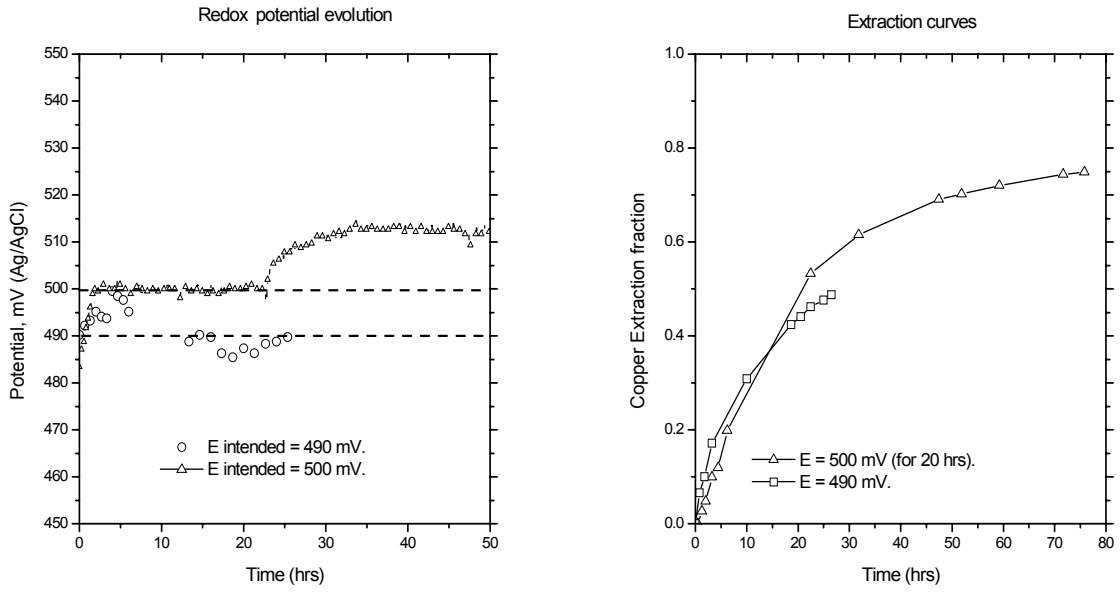

Figure 5.12 Similar extraction levels for two potential-controlled leaching scenarios.

5.4.3 Comparison between electrochemical and leaching experiments

Results from electrochemical tests performed on massive samples of chalcopyrite provide a first estimate of the dissolution rate based on mixed potential theory. Similarly, results from leaching tests can also provide values of dissolution rate by means of appropriate modeling of chalcopyrite leaching. The procedure to estimate dissolution rates from each tank leaching experiment is explained as follows.

The copper extraction is modeled after integration of Equation 5.12 as:

$$1-\overline{\overline{X}} = \int_{D_1}^{D_2}\left(1-\frac{2M}{\rho D_0}\int_0^t J_d^{leach}dt\right)^3 f(D_0)\,dD_0 \qquad (5.14)$$

where $f(D_0)$ corresponds to the PSD using the parameters estimated in Chapter 4 and J_d^{leach} is the dissolution rate estimated from experimental results of leaching which has to be compared to J_d^{elec} once they both are converted to current densities by Faraday's law and properly depicted by the Evans diagram from Figure 5.13.

Bouffard et al. (2006), have used equation 5.14 to estimate constant values of J_d^{leach} during pyrite oxidation by defining a constant "shrinkage rate". However, this is not applicable to the leaching of chalcopyrite, where the mineral surface is altered by passivity, and therefore, J_d^{leach} is a function of time. The estimation of this changing dissolution rate for different leaching tests was made by calculating values for the following defined function:

$$y(t) = \frac{2M}{\rho}\int_0^t J_d^{leach}\,dt \tag{5.15}$$

Equation 5.14 thus becomes:

$$1-\overline{\overline{X}} = \int_{D_1}^{D_2}\left(1-\frac{y(t)}{D_0}\right)^3 f(D_0)\,dD_0 \tag{5.16}$$

Values of $y(t)$ were adjusted and estimated by minimizing the difference between copper extractions predicted by Equation 5.16 and the experimental extraction values at time *t*. Once these values were obtained, the dissolution rate at each time was calculated by taking the local derivative:

$$J_d^{leach} = \frac{\rho}{2M}\left.\frac{\Delta y}{\Delta t}\right|_t \tag{5.17}$$

Figures 5.13 a) and c) show dissolution current density values and their evolution in time. It can be observed that constant values of the dissolution current density with time were estimated in the active region, and that, as passivity became more pronounced, current density profiles began to deviate at potentials higher than 480 mV.

Comparisons between leaching and electrochemical behavior can be established after obtaining dissolution current densities from leaching tests. Figure 5.13b shows two *E*-*J* curves for these two scenarios, where differences in the magnitude of dissolution current density along both curves range from 50 to 110 μA/cm^2. Luna-Sanchez et al. (2003) observed a greater discrepancy in this current density (dissolution rate) for acanthite leaching with cyanide solutions. In their study, the reaction velocity obtained from electrochemical experiments was three orders of magnitude larger than that

observed in actual cyanide leaching. They attributed this disagreement to dissimilar interfacial mechanisms operating in the two cases.

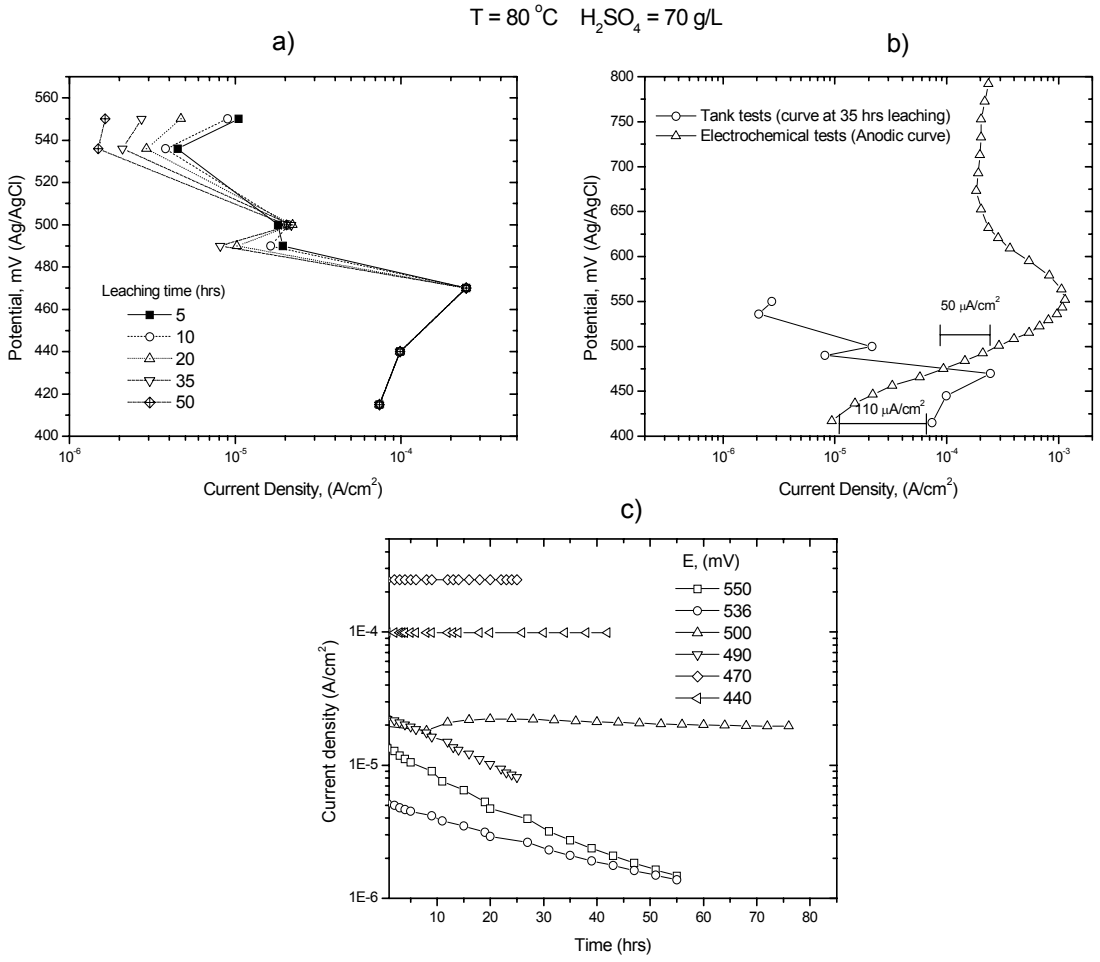

Figure 5.13 *E-J* relationships for chalcopyrite dissolution. a) Current density response for different times. b) Comparison between leaching and electrochemical behavior of current densities based on J_d^{elec} and J_d^{leach} respectively. c) Current density evolution in time

The discrepancy observed in the current density for electrochemical and leaching experiments of chalcopyrite in the present study was attributed to the poor estimation in the area of the electrodes used to carry out the electrochemical tests, since the cross-sectional area of routinely polished electrodes may have a roughness factor from 2 to 3

depending on the mode of polishing (Bard and Faulkner, 2001). It is clear that experimental errors influence the estimation of the dissolution current density from electrochemical techniques and lower dissolution rates are obtained.

5.4.4 Mathematical modeling of the leaching tests

The model developed in this work allows prediction of copper extraction levels for the passive and active regions based on the calibration of real tank leaching data. Parameters estimated from the calibration were used to simulate the effects of temperature and particle size distribution. Some relevant findings leading to the development of the model are outlined as follows:

1. The mathematical form for the chalcopyrite dissolution rate derived upon electrochemical considerations confirmed a similar dependency on reactant concentrations (conveniently expressed as the ferric-to-ferrous ratio) to that found for other sulfides such as chalcocite within regions where passivity does not occur.

2. Kinetic constant values were estimated from electrochemical and leaching tests and found to be similar in magnitude. Thus, the kinetic constant k_a' from leaching experiments is 35% greater than that estimated from anodic polarization studies. This result suggests that it is safe to assume a correlation between similar chemical and electrochemical environments.

3. The kinetic expression used in this work facilitated modeling of the effect of high potentials based on chemical changes in the leaching solution and the subsequent ferric species adsorption resulting in passivation. Current density variation at potentials higher than 470 mV, as shown in Figure 5.13c, suggests that time and potential changes are identified as the two possible types of leaching rate dependency. Time-dependent current density modeling is beyond the scope of this work. Instead, it was assumed that this current density variation is due to passivation occurring by means of species interactions with the chalcopyrite surface which are a function of solution potential.

4. Values estimated for adsorption energies for the leaching experiments were different from the value estimated from electrochemical tests. Indeed, parameter b_0 (from

Equation 5.10) directly related to the energies involved in the adsorption process was estimated and found to be dependent on solution potential. Several b_0 values estimated within the potential range from 415 to 550 mV are shown in Table 5.2. In the active region, up to 470 mV, values of b_0 are constant. However, as leaching is carried out at higher potentials, lower values of b_0 must be used in the kinetic model to obtain satisfactory fits.

Table 5.2 Values of the parameter b_0 estimated for the active and passive regions used for calibration of the kinetic leaching model.

Active region		Passive region	
E (mV)	b_0 (10^{10})	E (mV)	b_0 (10^{10})
415	1.05	490 to 500	1.045
440	1.05	536	0.388
470	1.05	550	0.059

Still, mixed potential theory proved useful as a qualitative approach to form the basis for the kinetic model including passivity and chemical species influencing mineral surface phenomena. The final expression in the form of mineral fraction unreacted incorporating parameters from electrochemical kinetics takes the following form:

$$\frac{dX}{dt} = \frac{6M}{\rho D_0} \frac{k'_a \left(\frac{C_{Fe^{3+}}}{C_{Fe^{2+}}} \right)}{\left(1 + B \left(\frac{C_{Fe^{3+}}}{C_{Fe^{2+}}} \right)^{\beta} C^n \right)} (1 - X)^{\frac{2}{3}} \tag{5.18}$$

where $k'_a = 1.35 \times 10^{-8}$ mol/s/cm^2.

The final equation used to simulate copper extraction assuming a Rosin-Rammler particle size distribution function is:

$$1 - \overline{\overline{X}} = \int_0^{\infty} \left(1 - \frac{t}{\tau(\xi)} \right)^3 m \xi^{m-1} \exp(-\xi^m) \, d\xi \tag{5.19}$$

where $\xi = D_0/D^*$, D^* is the 63.21% mass passing particle size, and the timescale is given thus:

$$\tau = \frac{\rho D^* \xi}{6M} \frac{\left(1 + B\left(\frac{C_{Fe^{3+}}}{C_{Fe^{2+}}}\right)^{\beta} C^n\right)}{k'_a\left(\frac{C_{Fe^{3+}}}{C_{Fe^{2+}}}\right)}$$

Parameters used for n and C as functions of potential were determined at 70 g/L H_2SO_4 and 80°C with the aid of speciation model:

$$n = 1 + \frac{2}{1 + \exp(0.0124E - 9.169)} \tag{5.20}$$

$$C = \frac{0.1219}{1 + \exp[-0.0355(E - 552.35)]} \tag{5.21}$$

and the following Nernst equation:

$$E = 545.6 + 29.3 \ln\left(\frac{C_{Fe^{3+}}}{C_{Fe^{2+}}}\right) \tag{5.22}$$

Figure 5.14 shows representations of copper extraction using the kinetic model Equation 5.19 for each leaching experiment. Good simulations were obtained for the active region up to 470 mV by merely using electrochemical parameters. However, extraction curves for potentials higher than 500 mV deviated from the model at leaching times longer than 40 hrs, possibly due to diffusion resistance through a layer of ferric precipitates.

5.4.5 Mathematical simulation of temperature and particle size effects

In order to simulate the effect of temperature Arrhenius equation was used to incorporate the temperature variation on the overall extraction rate:

$$\frac{k'_a(T)}{k'_a(80°C)} = \exp\left[-\frac{E_a}{R}\left(\frac{1}{T} - \frac{1}{353}\right)\right] \tag{5.23}$$

where E_a is the activation energy and corresponds to 83.7 kJ/mol based on the work of Munoz (1979).

Temperature-dependent parameters were also calculated from the speciation model at each temperature as shown in Table 5.3. Using these parameters and the activation energy value, levels of extraction can be simulated at different temperatures as shown in Figure 5.15. The baseline for all simulations corresponds to conditions of acid and total iron concentration already mentioned. Results of copper extraction at 80°C using the calibrated model were used for comparison with simulations at other temperatures. It can be observed that copper extraction increases abruptly as temperature changes from 60 to 80°C based on the use of an activation energy considering transport of electrons through elemental sulfur produced in accordance to reaction (I).

Table 5.3 Temperature-dependent parameters from the speciation model.

Temperature (^{o}C)	**60**	**70**	**80**
a	0.039	0.037	0.035
b	514.600	532.940	552.355
C_{max} (mol/L)	0.249	0.182	0.122
RT/*F* (mV)	26.55	28.06	29.30
E^0 (mV, Ag/AgCl)	509.86	526.59	541.91

The effect of particle size in different distributions was also simulated. Three cases were explored giving leaching rates under different particle size distributions characterized by the mean particle diameter μ. This parameter was calculated using the probability density function thus:

$$\mu = \int_{D_{\min}}^{D_{\max}} D_0 f(D_0) dD_0 \tag{5.26}$$

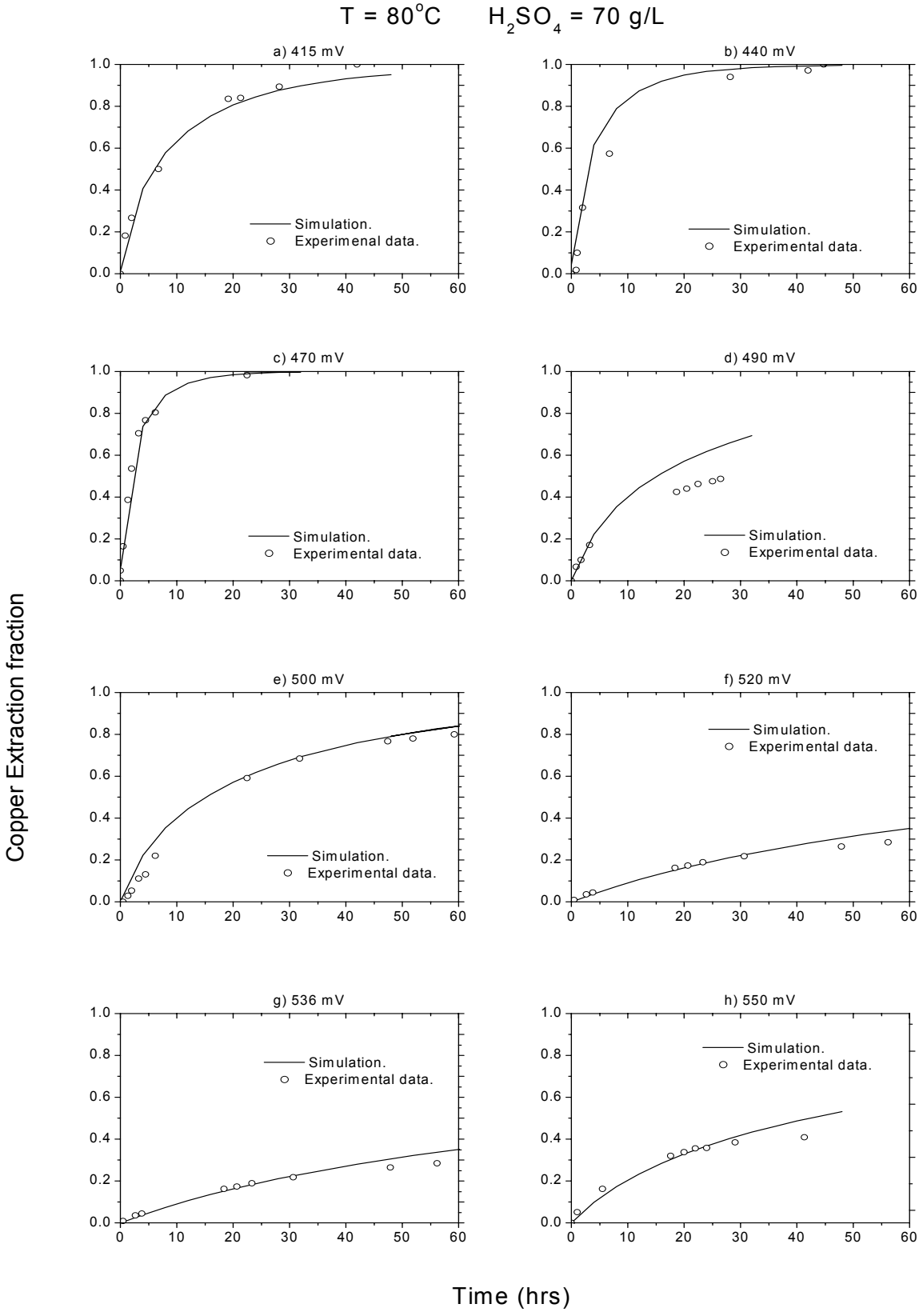

Figure 5.14 Tank leaching data and their respective representation with the mathematical model proposed in this study for both regions.

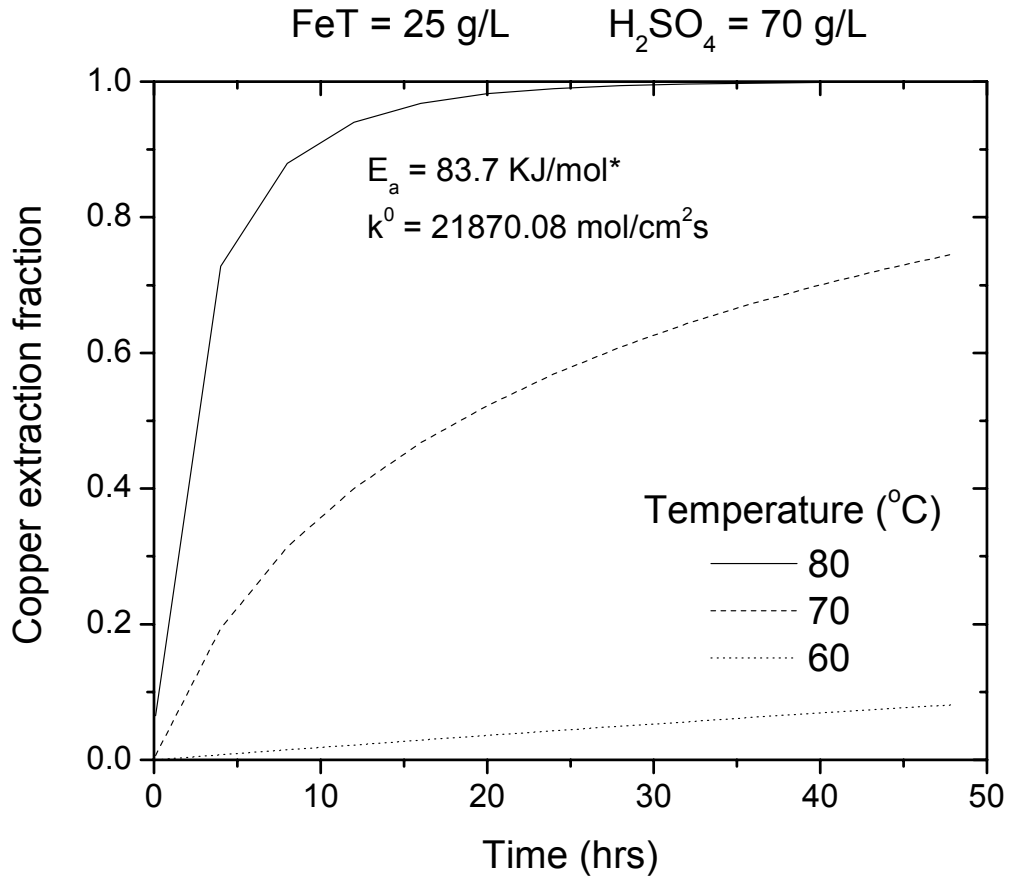

Figure 5.15 Temperature effect on leaching extraction rate.

Several extraction curves are plotted in Figure 5.16 for different particle size distributions. The Rosin-Rammler parameter *m* estimated from the PSD analysis discussed in Chapter 3 was used for all simulations given the negligible effect of *m* on extraction rate at constant *D** (which is similar to μ for large values of *m*). Simulation results clarify and confirm the role of particle size on the limits of extraction showing an inverse proportional relationship which has also been found among other researchers on chalcopyrite leaching where particle size effects have been experimentally investigated (Antonijevic et al., 2004; Munoz et al., 1979).

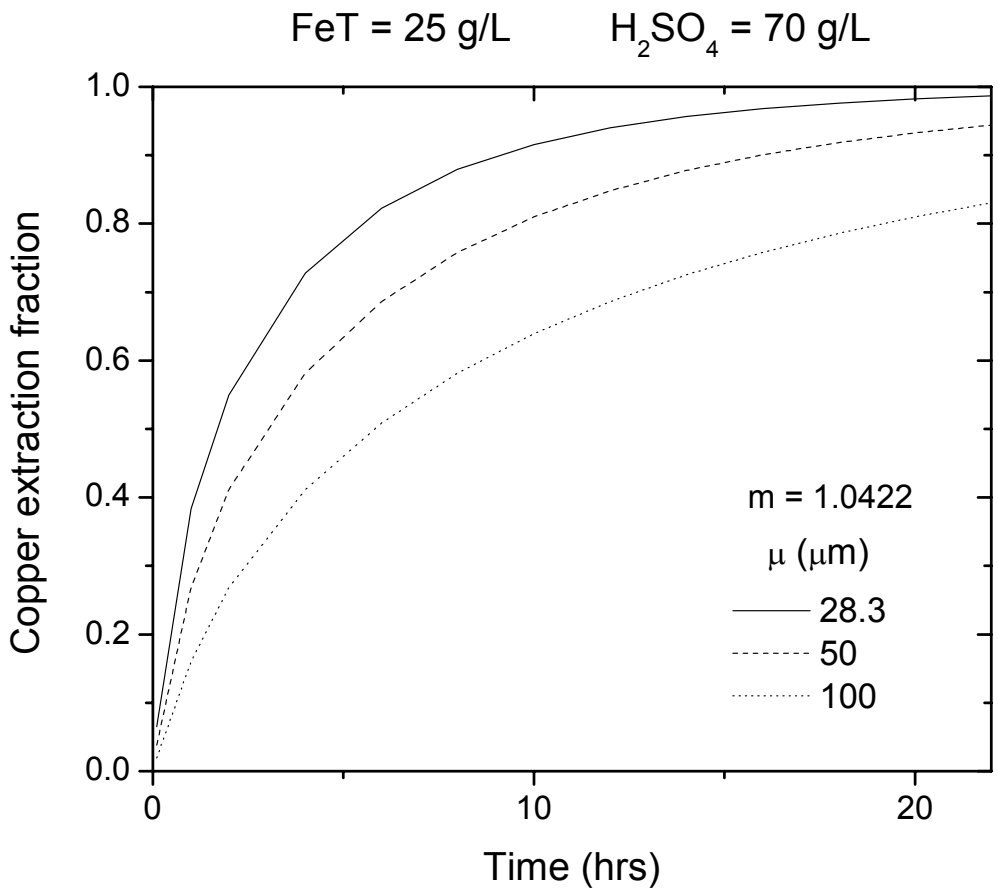

Figure 5.16 The effect of particle size distribution on leaching extraction rate.

CHAPTER 6 CONCLUSIONS

A systematic approach to characterize the kinetics of chalcopyrite leaching in atmospheric ferric sulfate solutions has been presented describing dissolution reaction rates over a wide redox potential range (from 415 to 550 mV Ag/AgCl). Solution thermodynamics of the leaching solution and electrochemical principles were used to develop a mathematical expression for modeling the dissolution reaction rate.

Ferric concentration dependency and passivity effects responsible for slowing down copper extraction at certain solution potentials were incorporated into the model. Thermodynamic considerations in the leaching solution support the mechanism of adsorption and precipitation of ferric species on the mineral surface causing passivation; calculations of chemical species concentrations and their role on the equilibrium solution potential were obtained with the aid of a speciation model. The model was calibrated using real solution potential data at different acidity levels.

Electrochemical rate theory was also used to describe the anodic and cathodic behavior of chalcopyrite. Potentiodynamic techniques were used to determine current density-potential relationships in the anodic region. Modeling of these curves was performed incorporating passivity effects associated to the solution chemistry. Effects of scanning rate, total iron content and ferric-to-ferrous ratio on the cathodic behavior were also explored. The ferric-to-ferrous ratio was identified as the most important variable, since it determines the redox potential corresponding to the potential at which chalcopyrite is dissolved (the mixed potential). On the other hand, scanning rate and total iron content were considered unimportant in identifying the dissolution rate as long as the rest anodic potential value is located in the vicinity of the equilibrium ferric reduction potential.

In order to correlate dissolution rates in the leaching experiments with measures of reactant concentration during validation of the model, redox potential values were taken as the average potential in well-controlled potential tests, or alternatively as the highest potential attained in the leaching solution in the passive region, since it was postulated that passivity occurs irreversibly when leaching is carried out at potentials higher than 470 mV (passivation potential). Once the potential exceeded this value no significant

increase of leaching rates was observed, even when the potential decreased again over the course of leaching.

The precipitation of jarosites or other ferric-bearing precipitates has been postulated to be the main reason of passivity, as opposed to the formation of a diffusion-resistant layer of elemental sulfur. However, it has also been stated that some type of diffusion mechanism might be responsible for the decrease observed in leaching results at regions of severe passivity. Separate analyses of dissolution current density from electrochemical and chemical environments showed that these values differ by a factor of 0.5 which was attributed to inaccurate determination of working surface areas on the electrodes used to perform electrochemical tests.

The mathematical model derived in this work incorporates kinetic parameters determined from electrochemical studies to simulate effects of ferric concentration on the dissolution rate. This model was able to represent real leaching data quite well in the active region up to the passivity potential of 470 mV. Although satisfactory results were not obtained in the simulation of the passive region by merely using constant adsorption energy values, instead observations of the passive behavior suggested the incorporation of adsorption energies as a function of leaching potential. Further research in the passive region with a view towards the development of a dynamic adsorption model could explain this adsorption energy variation in the passive region. Finally, simulation of temperature and particle size effects on the leaching of chalcopyrite gave results which followed the same trends observed by other researchers.

The kinetic model developed may help in the design of atmospheric ferric based leaching operations but beyond that purpose, the methodology adopted in this study opens up the possibility of predicting reaction rates based on the electrochemical characterization of different types of chalcopyrite that can successfully be correlated with their respective leaching behavior facilitated by the rigorous modeling of chalcopyrite leaching.

REFERENCES

Antonijevic, M.M., Bogdanovic, G.D., 2004. Investigation of the leaching of chalcopyritc ore in acidic solutions. Hydrometallurgy 73, 245–256.

Arslan, C., Arslan, F., 2003. Thermochemical review of jarosite and goethite stability regions at 25 and 95°C. Turkish J. Eng. Env. Sci. 27, 45–52.

Ballester, A., Cordoba, E., 2005. Hidrometalurgia de la calcopirita. Innovations in the hydrometallurgical processing of sulphides. Proceedings Hydrocopper 2005, Santiago, Chile.

Bard, A.J., Faulkner, L.R., 2001. Electrochemical Methods, Fundamentals and Applications. John Wiley & Sons, Inc., New York, NY.

Bolorunduro, S.A.., 1999. Kinetics of leaching of chalcocite in acid ferric sulfate media: Chemical and bacterial leaching. MASc Thesis, University of British Columbia.

Boon, M., Heijnen, J.J., 1993. Mechanisms and rate limiting steps in bioleaching of sphalerite, chalcopyrite and pyrite with *thiobacillus ferrooxidans*. Biohydrometallurgical Technologies, TMS, Warrendale, PA, 217–235.

Bouffard, S.C., Rivera-Vasquez, B.F. and Dixon, D.G., 2006. Leaching kinetics and stoichiometry of pyrite oxidation from a pyrite-marcasite concentrate in acid ferric sulfate media. Hydrometallurgy 84, 225–238.

Brown, S.L., Sullivan, J.D., 1934. Dissolution of various copper minerals, U.S. Bureau of Mines RI 3228.

Casas, J.M, Crisostomo G. and Cifuentes, L., 2005. Speciation of the Fe(II)-Fe(III)-H_2SO_4-H_2O system at 25 and 50°C. Hydrometallurgy 80, 254–264.

Casas, J.M, Crisostomo G. and Cifuentes, L., 2006. Dissolution of metallic copper in aqueous sulphuric acid-ferric sulphate solutions. Can. Metall. Q. 45, 243–248.

Crundwell, F.K., Godorr, S.A., 1997. A mathematical model of the leaching of gold in cyanide solutions. Hydrometallurgy 44, 147–162.

Davenport, W.G. and Biswas, A.K., 1976. Extractive Metallurgy of Copper, 4th ed., Pergamon Press, Oxford.

Dixon, D.G., 2003. Heap Leach modeling – the current state of the art. Proceedings Hydrometallurgy 2003, TMS, Warrendale, PA, 289–314.

Dixon, D.G., 2006. Modeling the atmosphelic leaching of copper sulfides. Short course, UBC Industrial Research Chair in Hydrometallurgy.

Dixon, D. G., Dreisinger, D. B., 2003. Hydrometallurgical process modeling for design and analysis, part II: Leaching kinetics and associated phenomena. EPD Congress 2002, TMS, Warrendale, PA, 687–708.

Dixon, D.G., Petersen, J., 2002. Thermophilic heap leaching of a chalcopyrite concentrate. Minerals Engineering 15, 777–785.

Dreisinger, D.B., 2006. Copper leaching from primary sulfides: Options for biological and chemical extraction of copper. Hydrometallurgy 83, 10–20.

Dry, M.J., Bryson, A.W., 1988. The prediction of redox potential in concentrated iron sulphate solutions. Hydrometallurgy 21, 59-72.

Duang, D.D., 1988. Adsorption Analysis: Equilibria and Kinetics. Imperial College Press, London.

Dutrizac, J.E., 1969. The kinetics of dissolution of synthetic chalcopyrite in aqueous acidic ferric sulfate solution. Trans. AIME 245, 955–959.

Dutrizac, J.E., 1989. Elemental sulphur formation during the ferric sulphate leaching of chalcopyrite. Can. Metall. Q. 28, 337–344.

Grifin, G.L., 1984. A simple phase transition model for metal passivation kinetics. J. Electrochem. Soc. 131, 18–21.

Gupta, C.K., Mukherjee, T.K., 1990. Hydrometallurgy in extraction processes, vol. I, CRC Press, Boca Raton, FL.

Hackl, R.P., Dreisinger, D.B., Peters, E. and King, J.A., 1995. Passivation of chalcopyrite during oxidative leaching in sulfate media. Hydrometallurgy 39, 25–48.

Hirato T., Majima, H. and Awakura, Y., 1987. The leaching of chalcopyrite with ferric sulfate. Metall. Trans. 18B, 489–496.

Hiroyoshi, N., Miki, H., Hirajima, T. and Tsunekawa, M., 2000. A model for ferrous-promoted chalcopyrite leaching. Hydrometallurgy 57, 31–38.

Jansen, R. and Beck, F., 1995. A kinetic model for the potentiodynamic passivation of zinc in acids or concentrated salt solutions. J. Electroanalytical Chem. 384, 93–97.

Jones, D.L. and Peters, E., 1976. The leaching of chalcopyrite with ferric sulfate and ferric chloride. Extractive Metallurgy of Copper, vol. 2, Hydrometallurgy and Electrowinning. AIME, New York, NY, 633–653.

Kametani, A. and Aoki, A., 1985. Effect of suspension potential on the oxidation rate of copper concentrate in a sulfuric acid. Metall. Trans. 18B, 489–496.

Li, J., Zhong, T.K. and Wadsworth, M.E., 1992. Application of mixed potential theory in hydrometallurgy. Hydrometallurgy 29, 47–60.

Liddell, K.C. and Bautista, R.G., 1981. A partial equilibrium chemical model for the dump leaching of chalcopyrite. Metall. Trans. 12B, 627–637.

Luna-Sanchez, R.M., Gonzalez, I. and Lapidus, G.T., 2003. A comparative study of silver sulfide oxidation in cyanide media. J. Electrochem. Soc. 150, D155–D161.

Madsen, B.W. and Wadsworth, M.E., 1981. A mixed kinetics dump leaching model of ores containing a variety of copper sulfide minerals. U.S. Bureau of Mines RI 8547.

Munoz, P.B., Miller, J.D. and Wadsworth, M.E., 1979. Reaction mechanism for the acid ferric sulfate leaching of chalcopyrite. Metall. Trans. 10B, 149–158.

Nava, D. and Gonzalez, I., 2006. Electrochemical characterization of chemical species formed during the electrochemical treatment of chalcopyrite in sulfuric acid. Electrochimica Acta 51, 5295–5303.

Nicol, M.J. and Lazaro I., 2002. The role of E_h measurements in the interpretation of the kinetics and mechanisms of the oxidation and leaching of sulphide minerals. Hydrometallurgy 63, 15–22.

Ogbonna, N., Petersen, J. and Dixon, D.G., 2005. HeapSim – Unraveling the mathematics of heap bioleaching. Computational Analysis in Hydrometallurgy, CIM, Montreal, QB, 225–239.

Parker. A., Klauber, C., Kougianos, A., Watling, H.R. and van Bronswijk, W., 2003. An X-ray photoelectron spectroscopy study of the mechanism of oxidative dissolution of chalcopyrite. Hydrometallurgy 71, 265–276.

Paul, B.C., Sohn, H.Y. and McCarter, M.K., 1992. Model for ferric sulfate leaching of copper ores containing a variety of sulfide minerals: Part 1. Modeling uniform size ore fragments. Metall. Trans. 23B, 537–548.

Petersen, J., Watling, H., Dixon, D.G., Franzmann, P., Plumb, J., Johnson, J., Harrison, S.T.L. and Hansford, G., 2005. Progress on the development of comprehensive understanding and a model of copper heap bioleaching – the AMIRA P768 project. HydroCopper 2005, Universidad de Chile, Santiago, 333–342.

Petersen, J., Dixon, D.G., 2003. The dynamics of chalcocite heap bioleaching. Hydrometallurgy 2003, TMS, Warrendale, PA, 351–364.

Petersen, J., Dixon, D.G., 2006. Competitive bioleaching of pyrite and chalcopyrite. Hydrometallurgy 83, 40–49.

Pinches, A., Myburgh, P.J. and van der Merwe, C., 2001. Process for the rapid leaching of chalcopyrite in the absence of catalysts. U.S. Patent 6,277,341.

Roine, A., 2002. HSC Chemistry v5.11 Database. Outokumpu Research Oy, Pori Finland.

Rush, B. and Newman, J., 1995. Periodic behavior in the iron-sulfuric acid system. J. Electrochem. Soc. 142, 3770–3779.

Sandstrom, A., Shchukarev, A. and Paul, J., 2005. XPS characterization of chalcopyrite chemically and bio-leached at high and low redox potential. Minerals Engng 18, 505–515.

Smith, C.L., Pike, R.W. and Murrill, P.W., 1970. Formulation and Optimization of Mathematical Models. International Textbook Company, Scranton, PA.

Stipp, S.L., 1990. Speciation in the Fe(II)-Fe(III)-SO_4-H_2O system at 25°C and low pH: Sensitivity of an equilibrium model to uncertainties. Environ. Sci. Technol. 24, 699–706.

Stott, M.B., Watling, H.R., Franzmann, P.D. and Sutton, D., 2000. The role of iron-hydroxy precipitates in the passivation of chalcopyrite during bioleaching. Minerals Engng. 13, 1117–1127.

Third, K.A., Cord-Ruwisch, R. and Watling, H.R., 2002. Control of the redox potential by oxygen limitation improves bacterial leaching of chalcopyrite. Biotech. Bioengng. 78, 443–441.

Tshilombo, A.F., 2004. Mechanism and kinetics of chalcopyrite passivation and depassivation during ferric and bacterial leaching. PhD thesis. The University of British Columbia.

Trejo-Gallardo, J., Viramontes-Gamboa, G. and Dixon, D.G., 2007. A thermodynamic model of chalcopyrite passivation. Submitted to Hydrometallurgy.

Viramontes-Gamboa, G., Rivera-Vasquez, B.F. and Dixon, D.G., 2007. The active-passive behavior of chalcopyrite: comparative study between electrochemical and leaching responses. J. Electrochem. Soc. 154, C299–C311.

Wadsworth, M.E., 1972. Advances in the leaching of sulphide minerals. Minerals Sci. Engng. 4, 36–47.

Warren, G.W., Wadsworth, M.E. and El-Raghy, S.M., 1982. Passive and transpassive anodic behavior of chalcopyrite in acid solutions. Metall. Trans. 13B, 571–579.

Watling, H.R., 2006. The bioleaching of sulphide minerals with emphasis on copper sulphides – a review. Hydrometallurgy 84, 81–108.